

International Journal of Modern Physics E
 © World Scientific Publishing Company

Polarization phenomenon in heavy-ion collisions

Takafumi Niida

*Department of Physics, University of Tsukuba, 1-1-1 Tennodai
 Tsukuba, Ibaraki 305-8571, JAPAN
 niida.takafumi.fw@u.tsukuba.ac.jp*

Sergei A. Voloshin

*Department of Physics and Astronomy, Wayne State University, 666 W. Hancock
 Detroit, Michigan 48201, USA
 sergei.voloshin@wayne.edu*

Received 16 April 2023

The strongly interacting system created in ultrarelativistic nuclear collisions behaves almost as an ideal fluid with rich patterns of the velocity field exhibiting strong vortical structure. Vorticity of the fluid, via spin-orbit coupling, leads to particle spin polarization. Due to the finite orbital momentum of the system, the polarization on average is not zero; it depends on the particle momenta reflecting the spatial variation of the local vorticity.

In the last few years, this field experienced a rapid growth due to experimental discoveries of the global and local polarizations. Recent measurements triggered further development of the theoretical description of the spin dynamics and suggestions of several new mechanisms for particle polarization. In this review, we focus mostly on the experimental results. We compare the measurements with the existing theoretical calculations but try to keep the discussion of possible underlying physics at the qualitative level. Future measurements and how they can help to answer open theoretical questions are also discussed. We pay a special attention to the employed experimental methods, as well as to the detector effects and associated corrections to the measurements.

Keywords: polarization; vorticity; nuclear collisions.

PACS numbers:

Contents

1. Introduction: Polarization as a collective phenomenon	2
2. Global and local polarizations	4
2.1. Nonrelativistic vorticity and the global polarization, $\langle P_{-y} \rangle$	4
2.2. Role of the magnetic field	6
2.3. Anisotropic flow and polarization along the beam direction	7
2.4. Circular polarization, P_ϕ ; polarization along x -direction, P_x	9
3. Spin and polarization in hydrodynamic description	10
3.1. Kinematic vorticity, thermal gradients, acceleration	10

2 *T. Nida and S. Voloshin*

3.2.	Shear-induced polarization and the spin Hall effect	11
3.3.	Additional comments	12
4.	How is it measured	13
4.1.	Self-analyzing weak decays of hyperons	13
4.1.1.	Multistrange hyperons and two-step decays	13
4.2.	Global polarization measurement	15
4.2.1.	Global polarization in which frame?	16
4.3.	Measuring polarization induced by anisotropic flow	16
4.4.	Feed-down effect	17
4.5.	Vector mesons spin alignment	17
4.6.	Detector acceptance effects	19
4.6.1.	Polarization along the initial angular momentum	19
4.6.2.	Polarization along the beam direction	20
4.6.3.	Acceptance effects in spin alignment measurements	21
5.	Overview of experimental results	22
5.1.	Global polarization of Λ hyperons	22
5.1.1.	Energy dependence	22
5.1.2.	Particle-antiparticle difference	23
5.1.3.	Differential measurements	25
5.2.	Global polarization of multi-strange hyperons	27
5.3.	Global spin alignment of vector mesons	29
5.4.	Polarization along the beam direction	31
6.	Open questions and future perspective	35
7.	Summary	36

1. Introduction: Polarization as a collective phenomenon

The discovery of the global polarization in heavy-ion collisions, the hyperon polarization along the system orbital momentum,^{1,2} followed by the measurements of the polarization along the beam direction,³ opened totally new opportunities for study of the nuclear collision dynamics and the properties of the quark-gluon plasma (QGP), as well as for deeper understanding of the spin and its transport in QGP medium. These polarization measurements are among the most significant discoveries made in heavy-ion collision program along with observations of the strong elliptic flow and jet quenching,⁴⁻⁷ and have generated intense theoretical discussions as well as experimental activities.

The phenomenon of the global polarization in heavy-ion collisions arises from the partial conversion of the orbital angular momentum of the colliding nuclei into the spin angular momentum of produced particles.⁸⁻¹⁰ As a result, the particles on average become polarized along the direction of the initial orbital momentum of the two colliding nuclei. The term “global” in the name of the phenomenon indicates that the component of the particle polarization along the system orbital momentum is not zero when averaged over all produced particles. The origin of the polarization

in heavy ion collisions is in the collective motion of the strongly interacting fluid, and it is unlikely to be related to the hyperon polarization (with respect to the production plane) observed in pp and pA collisions.¹¹

In a non-central nuclear collision, the most prominent pattern in the initial collective velocity distribution is a shear of the velocity field, $dv_z/dx \neq 0$, where the z direction is chosen along the beam, and the x direction is along the impact parameter vector defined as a vector connecting the centers of the two nuclei (pointing from the “target” to the “projectile” nucleus, the latter defined as the one moving in the positive z direction, see Fig. 1). Such a shear in the velocity field leads to nonzero vorticity characterizing the local orbital angular momentum density. Particle binary interactions in the system would have on average non-zero orbital angular momentum, which will be partially converted into spin of the final-state particles. For example, in a system with non-zero vorticity consisting of pions, the colliding pions have a preferential direction for their orbital angular momentum, and the spin of ρ mesons produced in such collisions ($\pi^+\pi^- \rightarrow \rho^0$) would point in that very direction.⁹

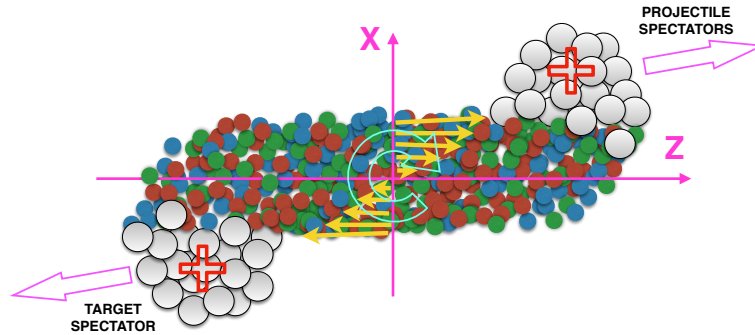


Fig. 1. Schematic view of a nuclear collision with x and z being the impact parameter and beam directions, respectively. The system orbital angular momentum as well as the magnetic field points into the page, opposite to the direction of the y axis. Solid yellow arrows indicate collective velocity field at $z = 0$. Open arrow indicates vorticity of the system.

The idea of the global polarization is almost 20 years old with the initial predictions for the quark and final particles polarization as high as “in the order of tens of a percent”.⁸ As pointed in Ref.,⁹ the global polarization phenomenon, if that strong, could affect the interpretation of different measurements. In particular, the polarization of the vector mesons would have a significant contribution to the elliptic flow measurements.^{9,12} The decay products of the vector resonances with spin pointing perpendicular to the reaction plane have the angular distribution enhancing the in-plane particle production and thus contributing to the elliptic flow measurements. The first measurements¹³ of the global polarization of Λ hyperons in Au+Au collisions at 200 GeV by the STAR Collaboration put an upper limit on hyperon polarization of $|P_\Lambda| \leq 0.02$. Subsequently, the theoretical predictions have

been improved¹⁴ to be consistent with these experimental results.

Particle polarization is determined by the vorticity of the fluid element where the particle has been produced. Due to the strong space-momentum correlation present in the system, the polarization of the particles in a certain momentum range would reflect the vorticity in the regions where those particles are predominantly emitted from. Thus, while averaged over the entire system only the “global” polarization component survives, the polarization in general depends on the particle momentum. Such polarization is often referred to as “local”. The non-trivial local vorticity can originate, for example, due to propagation of highly energetic jets produced by the partons hard scattering,^{15,16} or due to collective expansion of the system.^{17–20} An important example of that is the polarization along the beam direction due to (transverse) anisotropic flow, discussed first in Ref.¹⁸ on a basis of a simple Blast-Wave model, as well as observed in full hydrodynamical calculations.¹⁹

A short review format does not allow to describe and discuss in detail all the results and the questions under discussion. Our goal is to provide a more general picture of the field, to emphasize the major developments in our understanding of the phenomena and formulate outstanding questions, and to outline the relation of the current and future measurements to the underlying physics. In the first section of the review, we focus the discussion on the nature of the phenomenon. We use a very simple picture based on Glauber and Blast-Wave models for illustrations and rough estimates. Then we discuss the experimental side of the measurements, emphasizing the details important for the interpretation of the results and their uncertainties, as well as what is needed to accomplish this or other measurements. We proceed with an overview of available results and their current theoretical interpretations. The overview of the experimental results is followed by a summary of what we have learned so far, open questions, and future perspectives.

In the following discussion we refer to x , y , and z components of the polarization according to the coordinate system depicted in Figs. 1 and 2. In such a coordinate system, the global polarization would be given by the average of $-P_y = P_{-y}$, and the polarization along the beam direction is given by P_z . The global *averages* (over all particles and momenta) of P_z and P_x components (more exactly, the components of the total spin angular momentum) are expected to be zero.

2. Global and local polarizations

2.1. Nonrelativistic vorticity and the global polarization, $\langle P_{-y} \rangle$

A very significant development leading to a fast progress in this field was an application of the statistical methods to vortical fluid with non-zero spin particles,²¹ and development of the hydrodynamical calculations based on the assumption of the local angular momentum equilibrium.²² A rough estimate of the polarization

can be obtained with the help of a simple nonrelativistic ^a formula describing the particle distribution in a fluid with nonzero vorticity:²³

$$w \propto \exp \left[- \left(E + \boldsymbol{\omega}(\mathbf{s} + 1) - \frac{\mu}{s} \mathbf{s} \mathbf{B} \right) / T \right], \quad (1)$$

where $\boldsymbol{\omega} = \frac{1}{2} \nabla \times \mathbf{v}$ is the local vorticity of the fluid velocity (\mathbf{v}) field, \mathbf{B} is an external magnetic field, μ is the particle magnetic moment, and T is the temperature of the system at equilibrium. Then the polarization of particles with spin s is given by:

$$\mathbf{P} = \frac{\langle \mathbf{s} \rangle}{s} \approx \frac{(s + 1)}{3} \frac{(\boldsymbol{\omega} + \mu \mathbf{B} / s)}{T}. \quad (2)$$

For spin 1/2 particles, the vorticity contribution to the polarization is $P = \omega / 2T$ ^b. Averaged over the entire system volume, the vorticity direction coincides with the direction of the system orbital angular momentum. Note that the magnetic field created by fast positively charged nuclei is also pointing in the same direction.

Figure 1 shows a cartoon of a non-central nuclear collision with solid arrows indicating the velocity field of the matter at the plane $z = 0$. One can estimate the vorticity as $\omega_y \approx -\frac{1}{2} \partial v_z / \partial x$ where v_z is the net-velocity along the beam direction that depends on the number of participants coming from the target vs. projectile nuclei. The magnitude of v_z is reflected in the length of the solid arrows in Fig. 1. For a rough estimate of the vorticity, we present the velocity (v_z) distribution in the transverse plane in Fig. 2(a). In these calculations, the velocity was estimated as $v_z = (n_P - n_T) / (n_P + n_T)$ where n_P and n_T are the densities of the projectile and target nucleon participants (nucleons that experienced inelastic collisions) obtained by a simple Glauber model. The middle and right plots in Fig. 2 show the derivatives dv_z^* / dx and dv_z^* / dy (with the asterisks denoting the quantities in the rest frame of the fluid) weighted with the density of participating nucleons (roughly proportional to the produced particle density). From these estimates, one concludes that the vorticity might be as large as a few percent of fm^{-1} . Then the nonrelativistic formula (1) yields for the spin 1/2 particle polarization, $P \approx \omega / (2T)$, in the range of a few percent (assuming $T \sim 100$ MeV). Note that this simple estimate ignores the effect of nuclear transparency at high energies where the vorticity values could be significantly lower.

The vorticity of the system, especially its component along the system's orbital momentum, is directly related to the asymmetries in the initial velocity fields and thus it is intimately related to the directed flow v_1 .²⁴⁻²⁶ The v_1 is defined by the first Fourier moment $v_1 = \langle \cos(\varphi - \Psi_{RP}) \rangle$ of the produced particles' azimuthal

^aNote that for hyperons used in polarization measurements $m_H \gg T$, where T is the temperature and m_H is a hyperon mass.

^bThe nonrelativistic estimate can be also obtained by noting that the entropy $\sigma(E)$ of the rotating gas can be approximated as $\sigma(E - L^2 / (2I))$, where L is the orbital momentum, and I is the system inertia. Under condition of angular momentum conservation, $S + L = \text{const}$, this leads to $\partial \sigma / \partial S = L / (IT) = \omega / T$.

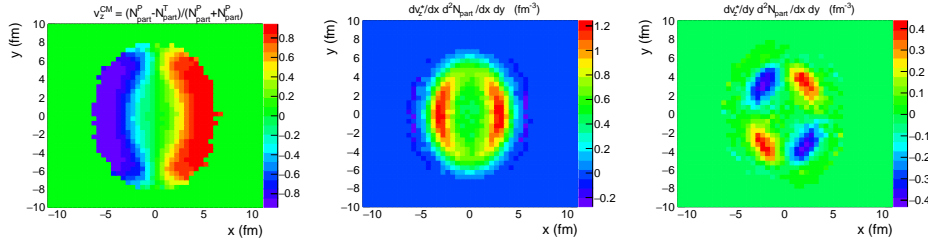
6 *T. Nida and S. Voloshin*


Fig. 2. (a) A transverse plane distribution of the z -component of the velocity of participant nucleons in the center-of-mass frame, (b) dv_z/dx distribution weighted with participant nucleon density, (c) the same for dv_z/dy , based on the Glauber model.

distribution relative to the collision reaction plane angle Ψ_{RP} . Hydrodynamic simulations show that the orbital angular momentum stored in the system and the directed flow of charged particles are almost directly proportional to each other.²⁶ This allows for an empirical estimate of the collision energy dependence of the global polarization.¹⁸ The STAR results for the directed flow^{27,28} and the hyperon global polarization^{1,2} from the RHIC Beam Energy Scan program show that the slopes of v_1 at midrapidity ($dv_1/d\eta$) for charged hadrons and the hyperon polarization are indeed strongly correlated. The charged-particle directed flow in Pb–Pb collisions at $\sqrt{s_{NN}} = 2.76$ TeV²⁹ is about three times smaller than at the top RHIC energy of 200 GeV.³⁰ This suggests that the global polarization at the LHC energies should be also about three times smaller than at RHIC and decreasing from $\sqrt{s_{NN}} = 2.76$ TeV to 5.02 TeV by about $\sim 20\%$.³¹ Even smaller polarization values at the LHC are expected when the directed flow is considered as a combination of the two effects – the tilt of the source in the longitudinal direction and the dipole flow originating from the asymmetry in the initial energy density distributions.³² Taking into account that only the contribution to the directed flow from the tilted source is related to the vorticity and that its contribution relative to the dipole flow decreases with the collision energy,³² one arrives to an estimate for the global polarization at the LHC energies of the order of 0.15–0.2 of that at the top RHIC energy.

2.2. Role of the magnetic field

In addition to possessing of the large orbital angular momentum, the system also experiences a strong magnetic field, of the order of $B \sim e/m_\pi^2 \sim 10^{14}$ T, generated in the initial state of the collision^{33–35} by the fast moving electrically charged nuclei and by the spectator protons after the collision. The direction of the magnetic field coincides with that of the orbital angular momentum. Therefore, the measured global polarization would include a contribution from the magnetic field, see Eq. (2), especially if the magnetic field is sustained for longer time by the presence of the QGP.³⁶ Unlike to the case for vorticity contribution, the contribution from the

magnetic field is opposite for particles and antiparticles because of the difference in signs of the magnetic moments μ in Eq. (2). The lifetime of the initial magnetic field depends on the electric conductivity of the QGP, which is poorly known. Precise measurements of the polarization difference between particles and antiparticles can provide an important constraint on the magnitude of the magnetic field at the hadronization time,^{23,37} as well as on medium conductivity. Such information is of particular importance for study of the chiral magnetic effect.³⁸

At lower collision energies, the passing time of two nuclei becomes larger and therefore the lifetime of the magnetic field is extended. Also, the medium created in the collision has positive net-charge due to baryon stopping. If the system with non-zero charge rotates, a magnetic field might be created at relatively later stage. Such late-stage magnetic fields may also contribute to the observed polarization.³⁹

In the global polarization picture based on the vorticity, one expects different particles to be polarized depending only on the particle spin in accordance with Eq. (2). A deviation could arise from effects of the initial magnetic field mentioned above, and from the fact that different particles are produced at different times or regions as the system freezes out,⁴⁰ or through meson-baryon interactions.⁴¹ Therefore, to understand the nature of the global polarization, it is crucial to measure the polarization of different particles, and if possible, particles with different spins. The polarization measurement with particles of different magnetic moments would provide additional information on the magnitude of the magnetic field. For example, the magnetic moment of Ω hyperon is three times larger than that of Λ hyperon ($\mu_{\Omega^-} = -2.02\mu_N$ and $\mu_{\Lambda} = -0.613\mu_N$ where μ_N is the nuclear magneton). Thus Ω hyperons are more sensitive to the magnetic field contribution to the polarization.

Comparing the polarization between particles and antiparticles, it might be important to account for the effects of non-zero baryon chemical potential,⁴² especially at lower collisions energies. Besides directly affecting the quark distributions, the non-zero chemical potential could lead to different freeze-out conditions, and thus to different effective vorticities responsible for the particle polarization. But overall such effects are expected to be relatively small.

2.3. Anisotropic flow and polarization along the beam direction

Anisotropic flow leads to non-trivial collective velocity fields in the transverse direction, which in its turn would manifest itself via particle polarization along the beam direction.¹⁸ The polarization P_z component dependence on the azimuthal angle would in general follow the anisotropic flow pattern of the same harmonic. We use a simple Blast Wave model to illustrate this phenomenon below.

In a simplest version of the Blast-Wave model including anisotropic flow,^{18,43,44} the particle production source at freeze-out is parameterized with 5 parameters: temperature T , maximum transverse radial flow velocity (rapidity) $\rho_{t,max}$ and amplitude of the azimuthal modulation in expansion velocity denoted as b_n , parameter R characterizing the size, and the spatial anisotropy parameter a_n . The source, see

8 *T. Niida and S. Voloshin*

Fig. 3(left), is then described by the following equations:

$$r_{max} = R[1 - a_n \cos(n\phi_s)], \quad \rho_t = \rho_{t,max} \left[\frac{r}{r_{max}(\phi_s)} \right] [1 + b_n \cos(n\phi_s)]. \quad (3)$$

It is assumed that the source element located at azimuthal angle ϕ_s is boosted with velocity ρ_t perpendicular to the surface of the source (ϕ_b). Note that the parameters a_n and b_n are usually small, $a_n, b_n < 0.1$, as follows from comparison of the model to the anisotropic flow and azimuthally sensitive femtosopic measurements.⁴⁵ In the limit of $a_n \ll 1$, $b_n \ll 1$, the longitudinal component of the vorticity can be written as:

$$\omega_z = \frac{1}{2}(\nabla \times \mathbf{v})_z \approx \left(\frac{\rho_{t,nmax}}{R} \right) \sin(n\phi_s)[b_n - a_n]. \quad (4)$$

It results in the following estimate for the hyperon polarization:

$$P_z \approx \frac{\omega_z}{2T} \approx 0.1 \sin(n\phi_s)[b_n - a_n], \quad (5)$$

where it is assumed that $\rho_{t,nmax} \sim 1$, $R \sim 10$ fm, and $T \sim 100$ MeV. In practice, the coefficients b_n and a_n are both of the order of a few percent,⁴⁵ often close to each other. That results in the magnitudes of z -polarization not greater than a few per-mill, almost an order of magnitude lower than what was obtained in original hydrodynamics calculations.¹⁹ Note that the estimate above is valid for anisotropic flow of any harmonics n .

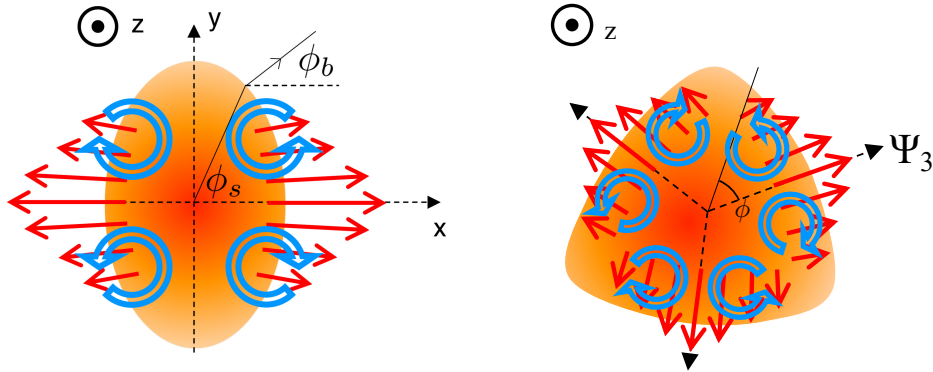


Fig. 3. Transverse plane schematic view of the system leading to elliptic (left) and triangular flow (right). Red solid arrows indicate the expansion velocity, the largest along the greatest density gradients defining the flow angles, Ψ_2 (coincides with x -axis) and Ψ_3 . In the left sketch, ϕ_s denotes azimuthal angle of the source element which is boosted to ϕ_b direction. Blue open arrows indicate local vorticities induced by the anisotropic flow.

2.4. Circular polarization, P_ϕ ; polarization along x -direction, P_x

Non-uniform stopping in the transverse plane, and dependence of the expansion velocity on rapidity leads to toroidal structure of the velocity field.^{20,46} Theoretical calculations suggest that a vortex ring could be created at very forward/backward regions, most prominent in the central collisions. Even a better pronounced vortex ring could be created when smaller object passes through larger object such as central asymmetric collisions of Cu+Au, d+Au, and p+Au as first proposed in Ref.,¹⁸ see Fig. 4. The calculations⁴⁷ show that the polarization due to such vortex rings could reach values as high as a few percent. The smaller object could be replaced with a jet instead of nuclei.¹⁶ According to the simulation of jet interacting with medium,^{15,48} vortex rings can be created around the path which jet passes through in the medium.

The axis of such a vortex ring is along the azimuthal direction relative to the smaller-nucleus-going or jet-going direction. The expected polarization in case of central A+B collisions can be expressed as $P_\phi \propto \hat{p}_T \times \hat{z}$ where \hat{p}_T and \hat{z} are the unit vectors along the particle transverse momentum and the beam direction, respectively (replace \hat{z} with a unit vector pointing along the jet axis in case for the jet-induced polarization). Such measurement would require a careful treatment of the detector acceptance effects, excluding left-right asymmetry in particle reconstruction.

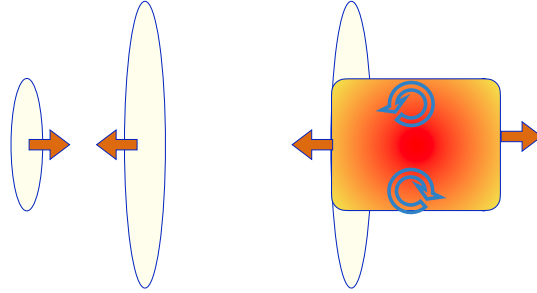


Fig. 4. A schematic view of a central asymmetric collision, such as Cu+Au, before (left) and after (right) the collision. The blue open arrows indicate the vorticity at the outer edges of the collision zone.

Finally we note the importance of the polarization measurements along the impact parameter direction, P_x . Theoretical models^{20,49} suggest that P_x has an azimuthal dependence following $\sin(2\phi)$ curve where ϕ is the hyperon's azimuthal angle relative to the reaction plane. Such a dependence on the azimuthal angle is also expected from simple calculations based on the Glauber model, see right panel in Fig. 2 where $\omega_x \propto \frac{1}{2} \partial v_z / \partial y$. This component could also have a contribution from the so-called shear induced polarization, see the discussion in Sec. 3.2. Similarly to

the P_ϕ measurements, these measurements could be technically difficult accounting for the acceptance effect.

3. Spin and polarization in hydrodynamic description

3.1. Kinematic vorticity, thermal gradients, acceleration

The Blast Wave model described in Sec. 2.3 is likely a gross oversimplification of the reality. It accounts, though still approximately, only for the contribution from so-called kinematic vorticity neglecting several other potentially important contributions. At the same time, as we discuss below, it describes surprisingly well the main features of the data. In relativistic hydrodynamics, the mean spin vector of $s = 1/2$ particles with mass m and four-momentum p is given by the following equation:²²

$$S^\mu(x, p) = -\frac{1}{8m}(1 - n_F)\epsilon^{\mu\tau\rho\sigma}p_\tau\varpi_{\rho\sigma}, \quad (6)$$

where n_F is the Fermi-Dirac distribution and ϖ is the *thermal vorticity* defined as:

$$\varpi_{\mu\nu} = \frac{1}{2}[\partial_\nu(u_\mu/T) - \partial_\mu(u_\nu/T)]; \quad (7)$$

$u_\mu = (\gamma, \gamma \mathbf{v})$ is the fluid 4-velocity (γ is the gamma factor), and T is the proper temperature. Thermal vorticity can be subdivided into two parts - the part including the temperature gradients $\partial_\mu(1/T)$ and the part proportional to the kinematic vorticity $\omega_{\mu\nu}^K = \frac{1}{2}(\partial_\nu u_\mu - \partial_\mu u_\nu)$. The latter in its turn can be separated into the part proportional to the acceleration and the spatial (transverse) part:

$$\omega_{\mu\nu}^K = \frac{1}{2}(A_\mu u_\nu - A_\nu u_\mu) + \frac{1}{2}(\nabla_\nu u_\mu - \nabla_\mu u_\nu), \quad (8)$$

where the acceleration vector $A^\mu = Du^\mu$ ($D = u^\nu \partial_\nu$ is the co-moving time derivative) and the $\nabla_\mu = \partial_\mu - u_\mu D$ is the so-called ‘‘orthogonal’’ (to u^μ) derivative. The transverse part of the kinematic vorticity can be also expressed via the vorticity (angular velocity) vector

$$\omega^\mu = \frac{1}{2}\epsilon^{\mu\nu\rho\sigma}u_\nu\partial_\rho u_\sigma, \quad (9)$$

as

$$\frac{1}{2}(\nabla_\nu u_\mu - \nabla_\mu u_\nu) = \epsilon_{\mu\nu\rho\sigma}\omega^\rho u^\sigma. \quad (10)$$

Using these notations and combining everything together, the spin vector can be written as

$$S^\mu(x, p) = \frac{1}{8m}(1 - n_F) \times \left[-\epsilon^{\mu\nu\rho\sigma}p_\sigma \frac{1}{T^2}(\partial_\nu T)u_\rho + 2 \frac{\omega^\mu(u^\nu p_\nu) - u^\mu(\omega^\nu p_\nu)}{T} - \frac{1}{T}\epsilon^{\mu\nu\rho\sigma}p_\sigma A_\nu u_\rho \right], \quad (11)$$

with three terms describing contributions of the temperature gradient, the vorticity, and the acceleration, respectively. Note that in an ideal uncharged fluid the temperature gradient term and the acceleration contribution are related by the equation of motion $\nabla_\mu T = T A_\mu$.

It is instructive to rewrite the expression Eq. 12 in the rest frame of the fluid, where $u^\mu = (1, 0, 0, 0)$, $D = \partial^t$, $\nabla_\mu = (0, \nabla)$, and $\omega^\mu = (0, \boldsymbol{\omega})$:

$$S^0(x, p) = \frac{1}{8m}(1 - n_F) \frac{\boldsymbol{\omega} \cdot \mathbf{p}}{T}, \quad (12)$$

$$\mathbf{S}(x, p) = \frac{1}{8m}(1 - n_F) \left(-\frac{\mathbf{p} \times \nabla T}{T^2} + 2 \frac{E \boldsymbol{\omega}}{T} + \frac{\mathbf{p} \times \mathbf{A}}{T} \right). \quad (13)$$

In the above expressions, E and \mathbf{p} are the energy and momentum of the particle in the fluid rest frame. In the nonrelativistic limit, the contribution related to the angular velocity (coinciding with nonrelativistic vorticity) is the largest, with the contribution from temperature gradients and acceleration being suppressed by v/c powers.

For completeness we also present an equation for the average spin vector transformation

$$\mathbf{S}^* = \mathbf{S} - \frac{\mathbf{p} \cdot \mathbf{S}}{E(E + m)} \mathbf{p}, \quad (14)$$

which should be used for calculation of the spin vector in the particle rest frame.

3.2. Shear-induced polarization and the spin Hall effect

Very recently two groups^{50,51} independently reported a new mechanism for the spin polarization - so called ‘‘shear induced polarization’’ (SIP) originated in symmetric part of the velocity gradients $\xi^{\mu\nu} = 1/2(\partial^\mu u^\nu + \partial^\nu u^\mu)$. Note that the expression for the polarization due to symmetric part of the velocity gradient tensor obtained by two groups are similar but not exactly the same with one qualitative difference as that the expressions obtained in Ref.⁵¹ explicitly depends on the freeze-out hypersurface shape, while the expression in Ref.⁵⁰ allows ‘‘local’’ interpretation. For our qualitative discussion of the effect below we will use the definition in Ref.⁵⁰

The origin of SIP is the motion of a particle in anisotropic fluid. It is zero if the particle is moving with the fluid velocity, which is in contrast to the polarization due to vorticity. It is clearly seen if the corresponding expressions are written in the fluid rest frame $u^\mu = (1, 0, 0, 0)$:

$$S_i^{(\text{vort})} \approx \frac{E}{8mT} \epsilon_{ikj} \frac{1}{2} (\partial_k v_j - \partial_j v_k), \quad (15)$$

$$S_i^{(\text{shear})} \approx \frac{1}{4mTE} \epsilon_{ikj} p_k p_m \frac{1}{2} (\partial_j v_m + \partial_m v_j). \quad (16)$$

One can see that the SIP contribution to the polarization is suppressed by the order of $(p/E)^2$ compared to vorticity contribution and become zero for particles moving

with the fluid velocity. It was also pointed out recently that the chemical potential gradients could also contribute to the polarization. This contribution identified as the “spin Hall effect” (SHE).⁵² In the fluid rest frame :

$$S_i^{(\text{SHE})} \approx \frac{1}{4mE} \epsilon_{ikj} p_k \partial_j (\mu/T). \quad (17)$$

Similarly to SIP, the polarization due to the gradients in baryon chemical potential (SHE – spin Hall effect) is also suppressed by a power of p/E . The SHE might be important in particular for the interpretation of the difference in polarization of particles and antiparticles. Note that the role of chemical potential was also studied earlier in a different context with the conclusion that for nonrelativistic hyperons the effect is almost negligible.⁴² The new effects, both SIP and SHE, are related to the motion of the particle in anisotropic fluid, and thus expected to be small for nonrelativistic particles compared to the polarization due to vorticity. This is the main reason why the calculations that involve quark degree of freedom result in stronger effects compared to those where SIP and SHE contributions are calculated directly for (nonrelativistic) hyperons. We discuss this in more detail in relation to the experimental measurements of the polarization along the beam direction (P_z).

3.3. *Additional comments*

While several model calculations do show a significant contribution to the hyperon polarization from temperature gradients and acceleration, in our more qualitative discussion we mostly argue on the basis of the contribution from kinematic vorticity. The freeze-out temperature of the system is about ~ 100 MeV, and all the hyperons are nonrelativistic in the local fluid frame. For that reason we also often estimate the polarization in the fluid frame, although all the experimental measurements are performed in the particle rest frame. We do treat the hyperons as relativistic in the laboratory frame though, as the fluid collective motion is relativistic. The nonrelativistic treatment might fail if the final particle polarization is due to the coalescence of initially (during the system evolution before the hadronization) polarized (constituent) quarks, with masses that are only factor of 2–3 higher than the temperature.

All hydrodynamic calculations use the Cooper-Frye prescription⁵³ for the fluid freeze-out. This prescription has several known problems (see e.g., Refs.^{54,55}), which might be not very important for calculations of the particle spectra, but it is not known how good the Cooper-Frye prescription is for calculation of the polarization. In particular, the contributions from the temperature gradients and acceleration might be questionable, as the very concept of freeze-out assumes insignificance of those effect. Then, their contributions would be related to the corresponding relaxation times of the system. Note, that if found significant, the measurement of those effects might provide unique information about the velocity and temperature gradients at freeze-out, for which the particle spectra are mostly insensitive.

Vortical effects may also strongly affect the baryon dynamics of the system, leading to a separation of baryon and antibaryons along the vorticity direction (perpendicular to the reaction plane) – the so-called Chiral Vortical Effect (CVE).³⁸ The CVE is similar in many respect to the more familiar Chiral Magnetic Effect (CME) – the electric charge separation along the magnetic field. For reviews on those and similar effects, as well as the status of the experimental search for those phenomena, see Refs.^{38,56} For a reliable theoretical calculation of both effects, one has to know the vorticity of the created system as well as the evolution of (electro)magnetic field.

In view of the recent polarization measurements in ultra-relativistic heavy-ion collisions, note the discussion⁵⁷ of a physical meaning of the spin angular momentum in quantum field theory and relativistic hydrodynamics.

4. How is it measured

4.1. Self-analyzing weak decays of hyperons

The hyperon weak decays provide a most straightforward way to experimentally measure polarization of particles produced in heavy-ion collisions. Because of its parity-violating weak decay, the angular distribution of the decay products at the hyperon rest frame obeys the following relation:

$$\frac{dN}{d\Omega^*} = \frac{1}{4\pi} (1 + \alpha_H \mathbf{P}_H^* \cdot \hat{\mathbf{p}}_B^*), \quad (18)$$

where α_H is the hyperon decay parameter, \mathbf{P}_H^* is the hyperon polarization vector, and $\hat{\mathbf{p}}_B^*$ is the unit vector in the direction of the daughter baryon momentum, and the Ω is its solid angle. The asterisk is used to denote quantities in the hyperon rest frame. The decay parameter α_H reflects analyzing power in the measurement, it is different for different hyperons. In case of Λ hyperon decay of $\Lambda \rightarrow p + \pi^-$, the decay parameter is $\alpha_\Lambda = 0.732 \pm 0.014$.⁵⁸ The decay parameter for $\bar{\Lambda} \rightarrow \bar{p} + \pi^+$ is usually treated same as Λ , i.e., $\alpha_\Lambda = -\alpha_{\bar{\Lambda}}$, assuming that charge conjugation parity (CP) symmetry is conserved, although the world average data shows slightly higher value $\alpha_{\bar{\Lambda}} = -0.758 \pm 0.014$.⁵⁸ In this paper, we follow this convention unless it is specified in the figure. We also note that the recent studies^{59,60} indicate that α_Λ could be larger by a few percent compared to the aforementioned value (and be closer to $\alpha_\Lambda \approx \alpha_{\bar{\Lambda}}$), leading to a few % reduction of the measured polarization.

4.1.1. Multistrange hyperons and two-step decays

Multistrange hyperons such as Ξ and Ω decay in two steps. For example, in case of Ξ^- hyperon (spin-1/2), $\Xi^- \rightarrow \Lambda + \pi^-$ with subsequent decay $\Lambda \rightarrow p + \pi^-$. If Ξ^- is polarized, its polarization is partially transferred to the daughter Λ . Both steps in such a cascade decay are parity-violating and thus can be used for an independent measurement of the parent hyperon polarization. The decay parameter for $\Xi^- \rightarrow \Lambda + \pi^-$ is $\alpha_{\Xi^-} = -0.401 \pm 0.010$.⁵⁸ This value of α_{Ξ^-} was constrained by the

measurement of the product of $\alpha_{\Xi}\alpha_{\Lambda}$ with the α_{Λ} measured separately, therefore the change of α_{Λ} would affect the value of α_{Ξ} as well. We also note that the recent direct measurement of α_{Ξ} ⁵⁹ suggests a slightly different value ($\alpha_{\Xi} = -0.376 \pm 0.007$).

The polarization of the daughter baryon in the weak decay of a spin-1/2 hyperon is described by the Lee-Yang formula^{61–63} with three decay parameters; α , β , and γ , where α is a parity-violating part reflecting decay asymmetry as mentioned above, β accounts for the violation of the time reversal symmetry, and γ satisfies $\alpha^2 + \beta^2 + \gamma^2 = 1$. For a particular case of $\Xi \rightarrow \Lambda + \pi$ decay, the daughter Λ polarization in its rest frame can be written as:

$$\mathbf{P}_{\Lambda}^* = \frac{(\alpha_{\Xi} + \mathbf{P}_{\Xi}^* \cdot \hat{\mathbf{p}}_{\Lambda}^*)\hat{\mathbf{p}}_{\Lambda}^* + \beta_{\Xi}\mathbf{P}_{\Xi}^* \times \hat{\mathbf{p}}_{\Lambda}^* + \gamma_{\Xi}\hat{\mathbf{p}}_{\Lambda}^* \times (\mathbf{P}_{\Xi}^* \times \hat{\mathbf{p}}_{\Lambda}^*)}{1 + \alpha_{\Xi}\mathbf{P}_{\Xi}^* \cdot \hat{\mathbf{p}}_{\Lambda}^*}, \quad (19)$$

where $\hat{\mathbf{p}}_{\Lambda}^*$ is the unit vector of the Λ momentum, and Ξ polarization \mathbf{P}_{Ξ}^* is given in the Ξ rest frame. Averaging over the angular distribution of the daughter Λ in the rest frame of the Ξ given by Eq. (18) leads to

$$\mathbf{P}_{\Lambda}^* = C_{\Xi-\Lambda}\mathbf{P}_{\Xi}^* = \frac{1}{3}(1 + 2\gamma_{\Xi})\mathbf{P}_{\Xi}^*. \quad (20)$$

Using the measured value for the γ_{Ξ} parameter,^{58,63} the polarization transfer coefficient for Ξ^- to Λ decay leads to:

$$C_{\Xi-\Lambda} = \frac{1}{3}(1 + 2 \times 0.916) = +0.944. \quad (21)$$

This shows that the polarization of Ξ^- is transferred to daughter Λ almost at its full value. We also would like to point out that the value of the γ parameter is constrained by the measured α and ϕ as $\gamma = (1 - \alpha^2)\cos^2\phi$ where $\phi = \tan^{-1}\beta/\gamma$, therefore the change in α parameter as well as ϕ value would also lead to a change in the γ parameter.

The polarization of the daughter baryon in a two-particle decay of spin-3/2 hyperon, i.e., $\Omega \rightarrow \Lambda + K$, can be also described by three parameters α_{Ω} , β_{Ω} , and γ_{Ω} .⁶⁴ The decay parameter α_{Ω} determines the angular distribution of Λ in the Ω rest frame and is measured to be small:⁵⁸ $\alpha_{\Omega} = 0.0157 \pm 0.0021$; this means that the measurement of Ω polarization via analysis of the daughter Λ angular distribution is practically impossible. The polarization transfer in this decay is determined by the γ_{Ω} parameter as:^{64–66}

$$\mathbf{P}_{\Lambda}^* = C_{\Omega-\Lambda}\mathbf{P}_{\Omega}^* = \frac{1}{5}(1 + 4\gamma_{\Omega})\mathbf{P}_{\Omega}^*. \quad (22)$$

The parameter γ_{Ω} is unknown but considering the time-reversal violation parameter β_{Ω} to be small, one can expect that the unmeasured parameter γ_{Ω} is $\gamma_{\Omega} \approx \pm 1$, based on the constraint $\alpha^2 + \beta^2 + \gamma^2 = 1$. This results in a polarization transfer to be $C_{\Omega-\Lambda} \approx 1$ or $C_{\Omega-\Lambda} \approx -0.6$. As discussed later, the measurement of Ω global polarization can help to resolve the ambiguity of γ_{Ω} under assumption of the vorticity picture in heavy-ion collisions.

4.2. Global polarization measurement

Polarization component along the initial orbital angular momentum \mathbf{L} for hyperons, referred to as global polarization when averaged over all produced particles, can be obtained by integrating Eq. (18) over the polar angle of daughter baryon θ_B^* and the reaction plane angle Ψ_{RP} , considering the projection of the polarization onto the direction \mathbf{L} . In Eq. (18), $\mathbf{P}_H \cdot \hat{\mathbf{p}}_B^*$ can be substituted with $P_H \cos \theta^* = P_H \sin \theta_B^* \sin(\Psi_{\text{RP}} - \phi_B^*)$ where θ^* is the angle between the polarization vector and momentum of daughter baryon in the hyperon rest frame, and θ_B^* and ϕ_B^* are azimuthal and polar angles of daughter baryon in the hyperon rest frame. Then the average of $\sin(\Psi_{\text{RP}} - \phi_B^*)$ is calculated as

$$\begin{aligned} & \langle \sin(\Psi_{\text{RP}} - \phi_B^*) \rangle \\ &= \int d\Omega^* \int \frac{d\Psi_{\text{RP}}}{2\pi} \frac{1}{4\pi} [1 + \alpha_H P_H \sin \theta_B^* \sin(\Psi_{\text{RP}} - \phi_B^*)] \sin(\Psi_{\text{RP}} - \phi_B^*) \end{aligned} \quad (23)$$

$$= \frac{\alpha_H P_H}{2} \int d\Omega^* \sin \theta_B^*. \quad (24)$$

Hence, this leads to

$$\begin{aligned} P_H &= \frac{8}{\pi \alpha_H} \frac{1}{(4/\pi) \int d\Omega^* \sin \theta_B^*} \langle \sin(\Psi_{\text{RP}} - \phi_B^*) \rangle \\ &= \frac{8}{\pi \alpha_H} \frac{1}{A_0} \langle \sin(\Psi_{\text{RP}} - \phi_B^*) \rangle, \end{aligned} \quad (25)$$

where $A_0 = (4/\pi) \int d\Omega^* \sin \theta_B^*$ is an acceptance correction factor and usually estimated in a data-driven way. If the detector can measure all produced hyperons of interest, the factor A_0 becomes unity. In practice, A_0 slightly deviates from unity and depends on the event multiplicity and the hyperon transverse momentum p_T . Equation (25) does not account for the polarization dependence on azimuthal angle, but such a dependence as well as the presence of elliptic flow might affect the measurements. For a more detailed discussion of the acceptance and tracking efficiency corrections including P_H azimuthal dependence, see Sec. 4.6.

Experimentally the first-order event plane angle Ψ_1 is used as a proxy of Ψ_{RP} . Then Eq. (25) can be rewritten to take into account for the event plane resolution as follows¹³

$$P_H = \frac{8}{\pi \alpha_H} \frac{1}{A_0} \frac{\langle \sin(\Psi_1 - \phi_B^*) \rangle}{\text{Res}(\Psi_1)}, \quad (26)$$

where $\text{Res}(\Psi_1)$ is the event plane resolution defined as $\langle \cos(\Psi_1 - \Psi_{\text{RP}}) \rangle$. The azimuthal angle Ψ_1 can be determined by measuring spectator fragments and provides the direction of the initial orbital angular momentum.⁶⁷

Equation 26 provides a possibility to measure global polarization of hyperons by measuring only azimuthal distributions of the daughter baryon. While this approach based on well established anisotropic flow techniques, a slightly better statistical accuracy could be achieved by measuring the full angular distribution, including

polar angle. In this case,

$$P_H = \frac{3}{\alpha_H} \langle \cos \theta^* \rangle = \frac{3}{\alpha_H} \langle \sin \theta_B^* \sin(\Psi_{RP} - \phi_B^*) \rangle. \quad (27)$$

For a discussion of the acceptance and tracking efficiency corrections including the azimuthal dependence, see Sec. 4.6.

4.2.1. *Global polarization in which frame?*

As defined in Eq. (18), the polarization is measured in the hyperon rest frame and the global polarization is the polarization component along the orbital angular momentum \mathbf{L} direction in the center-of-mass frame of heavy-ion collisions as shown in Eq. (26). Strictly speaking, the \mathbf{L} direction in Λ rest frame is different from the \mathbf{L} direction in the center-of-mass frame of heavy-ion collisions, and therefore the proper treatment of the reference frame and measured polarization is needed. Reference⁶⁸ studies the effect of the frame difference in the measurement of global polarization and found that the effect is small and reaches about 10% for high transverse momentum ($p_T \sim 4\text{--}5$ GeV/ c). Note that the mean p_T for Λ is ~ 1 GeV/ c ⁶⁹ depending on the centrality and collision energy, and could be slightly higher ($p_T \sim 1.5$ GeV/ c) with the kinematic cut for Λ used in the polarization measurement.

4.3. *Measuring polarization induced by anisotropic flow*

As already mentioned in Sec. 2.3, one can expect that azimuthal anisotropic flow would lead to a vorticity pointing along the beam direction. The orientation, along or opposite to the beam, in this case depends on the azimuthal angle of the particle. Similarly to the case of the global polarization, the longitudinal component of the polarization P_z can be obtained by integrating Eq. (18) as $\int dN/d\Omega^* \cos \theta^* d\Omega^*$ in which $\mathbf{P}_H \cdot \hat{\mathbf{p}}_B^*$ is replaced by $P_z \cos \theta_B^*$, where θ_B^* is the polar angle of daughter baryon in the parent hyperon rest frame. This leads to

$$P_z = \frac{1}{A_z} \frac{3 \langle \cos \theta_B^* \rangle}{\alpha_H}, \quad (28)$$

where A_z is the acceptance correction factor (see Sec. 4.6.2). For the case of perfect detector acceptance, $A_z = 1$. The factor A_z can be calculated using the data and is known to weakly depend on the transverse momentum and collision centrality. For more details on the correction factors, see Sec. 4.6.

As follows from considerations in Sec. 2.3, see Eq. 4, the polarization induced by n -th harmonic anisotropic flow, if any, is expected to depend on the azimuthal angle of hyperons as $P_z(\phi) \propto \sin[n(\phi - \Psi_n)]$. Then such a polarization can be quantified by the corresponding Fourier coefficient

$$P_{z,sn} = \langle P_z \sin[n(\phi_H - \Psi_n)] \rangle, \quad (29)$$

where Ψ_n is n-th harmonic event plane. Then, similarly to the case for global polarization as in Eq. (26), Eq. (29) can be rewritten accounting for the event plane resolution

$$P_{z,sn} = \frac{\langle P_z \sin[n(\phi_H - \Psi_n)] \rangle}{\text{Res}(n\Psi_n)}, \quad (30)$$

where $\text{Res}(n\Psi_n)$ is the resolution of n-th harmonic event plane defined as $\langle \cos[n(\Psi_n^{\text{obs}} - \Psi_n)] \rangle$ (“obs” denotes an observed angle).

4.4. Feed-down effect

It is known that a significant amount of Λ and Ξ hyperons comes from decays of heavier particles, such as Σ^0 , Σ^* , and Ξ baryons for Λ , and $\Xi(1530)$ baryons for Ξ . While the secondary particles from weak decays can be reduced, though not completely, using information on the decay topology, particles decayed via strong interaction cannot be separated from primary particles experimentally due to their short lifetimes. If the parent particles are polarized, the polarization is transferred to the daughter hyperons with certain polarization transfer factor, as discussed with Eqs. 20 and 22. The transfer factor C depends on the type of decays and could be negative, for instance, $C_{\Sigma^0\Lambda} = -1/3$ for the electromagnetic decay of $\Sigma^0 \rightarrow \Lambda + \gamma$.²³ Based on model studies,^{23,49,70–72} such feed-down contribution is found to suppress the polarization of inclusively measured Λ compared to primary Λ by 10-20% depending on the model used. In case for Ξ hyperons, $\Xi(1530)$ has spin 3/2 and the polarization transfer factor in the decay of $\Xi(1530) \rightarrow \Xi^- + \pi$ is equal to unity. Therefore the feed-down contribution for Ξ leads to the enhancement of the polarization of inclusive Ξ by $\sim 25\%$.⁷²

Although the effect of feed-down is not so significant, it is important to assess the effect, especially when extracting physical quantities such as the vorticity and magnetic field at the freeze-out. Note that the feed-down correction relies on the assumption of local thermodynamic equilibrium for spin degree of freedom as formulated in Ref.²³ But it is not clear if the relaxation time is similar for the vorticity and magnetic field. Furthermore, actual situation may be more complicated since some of the particles have a shorter lifetime than the system lifetime (10–15 fm/c).

4.5. Vector mesons spin alignment

Vector mesons, $s=1$ particles, can be also utilized to study the particle polarization in heavy-ion collisions. Unlike in the case of hyperons’ weak decay, vector mesons predominantly decay via parity conserved (strong or electromagnetic) interaction. Therefore, one cannot determine the direction of the polarization of vector mesons, and their polarization state is usually reported via so-called spin-alignment measurements. The spin state of a vector meson is described by the spin density matrix ρ_{mn} . The diagonal elements of this matrix have a meaning of the probabilities for spin projections onto a quantization axis to have values 0, ± 1 ; ρ_{00} represents the

probability for the spin projection to be zero. As $s_z = \pm 1$ projections can not be distinguished, and the sum of the probabilities has to be unity, only one independent diagonal element, usually ρ_{00} , can be measured. In the case of vector meson decay into two (pseudo)-scalar mesons, ρ_{00} can be determined directly from the angular distributions of the vector mesons decay products (given by the squares of the corresponding spherical harmonics):

$$\frac{dN}{d\Omega^*} = \frac{3}{8\pi} [1 - \rho_{00} + (3\rho_{00} - 1) \cos^2 \theta^*], \quad (31)$$

where θ^* is the angle of one of the daughter particles with respect to the polarization direction in the rest frame of the vector meson. For the global spin alignment measurement, the polarization direction is given by the orbital angular momentum direction of the system, perpendicular to the reaction plane. In the case of unpolarized particles, ρ_{00} equals $1/3$. The deviation of ρ_{00} from $1/3$ would indicate spin alignment of vector mesons.

The spin alignment, $\Delta\rho = \rho_{00} - 1/3$, can be measured by directly analyzing $\cos^2 \theta^*$ distribution given in Eq. 31, or considering $\langle \cos^2 \theta^* \rangle$ as follows

$$\langle \cos^2 \theta^* \rangle = \int d\Omega^* \frac{3}{8\pi} [1 - \rho_{00} + (3\rho_{00} - 1) \cos^2 \theta^*] \cos^2 \theta^* = \frac{1}{3} + \frac{2}{5} \Delta\rho. \quad (32)$$

It results in

$$\Delta\rho = \frac{5}{2} \left(\langle \cos^2 \theta^* \rangle - \frac{1}{3} \right). \quad (33)$$

Taking also into account the event plane resolution⁷³ one arrives to the equation:

$$\rho_{00} = \frac{1}{3} + \frac{4}{1 + 3\text{Res}(2\Psi)} \left(\rho_{00}^{\text{obs}} - \frac{1}{3} \right), \quad (34)$$

where ρ_{00}^{obs} is the measured (“observed”) signal and $\text{Res}(2\Psi)$ is the event plane resolution defined as $\langle \cos[2(\Psi - \Psi_{\text{RP}})] \rangle$ where Ψ can be either the first-order or second-order event plane. One could also analyze the daughter product distribution relative to the reaction plane^{18,73} similarly to that performed in the global polarization measurement:

$$\rho_{00} = \frac{1}{3} - \frac{4}{3} \frac{\langle \cos[2(\phi^* - \Psi)] \rangle}{\text{Res}(2\Psi)}, \quad (35)$$

where ϕ^* is the azimuthal angle of the daughter product in the parent rest frame.

In the case of vector meson decaying into two fermions, e.g. $J/\psi \rightarrow e^+e^-$, the interpretation of the final angular distribution in terms of the vector meson polarization is less straightforward, as it involves the spin wave functions of the daughter fermions. In this case the angular distribution of the daughter particles is often parameterized with a set of lambda parameters. For the distribution integrated over azimuthal angle, it reduces to

$$\frac{dN}{d\cos\theta^*} \propto \frac{1}{3 + \lambda_\theta} [1 + \lambda_\theta \cos^2 \theta^*]. \quad (36)$$

The λ_θ parameter can be then determined from

$$\langle \cos^2 \theta^* \rangle = \frac{1 + 3\lambda_\theta/5}{3 + \lambda_\theta}. \quad (37)$$

If the masses of the fermions are small, the helicity conservation tells that they should be in the spin state with projection on their momentum ± 1 . In this case, λ_θ parameter is related to the probability for a vector meson to have spin projection zero via equation⁷⁴

$$\lambda_\theta = \frac{1 - 3\rho_{00}}{1 + \rho_{00}}. \quad (38)$$

4.6. Detector acceptance effects

4.6.1. Polarization along the initial angular momentum

We start with deriving the correction for polarization measurements based on Eq. 25. For the case of an imperfect detector, one has to take into account that in the calculation of the average $\langle \sin(\Psi_{\text{RP}} - \phi^*) \rangle$, the integral over solid angle $d\Omega^* = d\phi^* \sin \theta^* d\theta^*$ of the hyperon decay baryon's 3-momentum \mathbf{p}^* in the hyperon rest frame, is affected by detector acceptance:

$$\begin{aligned} \langle \sin(\Psi_{\text{RP}} - \phi^*) \rangle &= \int \frac{d\Omega^*}{4\pi} \frac{d\phi_H}{2\pi} A(\mathbf{p}_H, \mathbf{p}^*) \int_0^{2\pi} \frac{d\Psi_{\text{RP}}}{2\pi} \{1 + 2v_{2,H} \cos[2(\phi_H - \Psi_{\text{RP}})]\} \\ &\quad \times \sin(\Psi_{\text{RP}} - \phi^*) [1 + \alpha_H P_H(\mathbf{p}_H; \phi_H - \Psi_{\text{RP}}) \sin \theta^* \cdot \sin(\Psi_{\text{RP}} - \phi^*)]. \end{aligned} \quad (39)$$

Here \mathbf{p}_H is the hyperon 3-momentum, and $A(\mathbf{p}_H, \mathbf{p}_p^*)$ is a function to account for detector acceptance. The integral of this function over $(d\Omega_p^*/4\pi)(d\phi_H/2\pi)$ is normalized to unity. The polarization component along the system orbital angular momentum could depend on the relative azimuthal angle $(\phi_H - \Psi_{\text{RP}})$. Taking into account the symmetry of the system, one can expand the polarization as a function of $(\phi_H - \Psi_{\text{RP}})$ in a sum over even harmonics. Keeping below only the first two terms:

$$P_H(\phi_H - \Psi_{\text{RP}}, p_t^H, \eta^H) = P_0(p_t^H, \eta^H) + 2P_2(p_t^H, \eta^H) \cos[2(\phi_H - \Psi_{\text{RP}})]. \quad (40)$$

Substituting it into Eq. 39 and integrating over Ψ_{RP} one gets

$$\begin{aligned} \langle \sin(\Psi_{\text{RP}} - \phi^*) \rangle &= \frac{\alpha_H}{2} \int \frac{d\Omega^*}{4\pi} \frac{d\phi_H}{2\pi} A(\mathbf{p}_H, \mathbf{p}^*) \sin \theta^* \\ &\quad \times [(P_0 + 2P_2 v_2) - (P_2 + P_0 v_2) \cos[2(\phi_H - \phi^*)]] \\ &= \frac{\alpha_H \pi}{8} [A_0(P_0 + 2P_2 v_2) - A_2(P_2 + P_0 v_2)], \end{aligned} \quad (41)$$

where the ‘‘acceptance’’ functions $A_0(p_t^H, \eta^H)$ and $A_2(p_t^H, \eta^H)$ are defined by:

$$A_0(p_t^H, \eta^H) = \frac{4}{\pi} \int \frac{d\Omega^*}{4\pi} \frac{d\phi_H}{2\pi} A(\mathbf{p}_H, \mathbf{p}^*) \sin \theta^*. \quad (42)$$

$$A_2(p_t^H, \eta^H) = \frac{4}{\pi} \int \frac{d\Omega^*}{4\pi} \frac{d\phi_H}{2\pi} A(\mathbf{p}_H, \mathbf{p}^*) \sin \theta^* \cos[2(\phi_H - \phi^*)]. \quad (43)$$

20 *T. Niida and S. Voloshin*

For the perfect acceptance $A_0 = 1$ and $A_2 = 0$. Similarly one obtains:

$$\begin{aligned} & \langle \sin(\Psi_{\text{RP}} - \phi^*) \cos[2(\phi_H - \phi^*)] \rangle \\ &= \frac{\alpha_H \pi}{8} \left[A_0 (P_2 + P_0 v_2) - \frac{1}{2} A_2 (P_0 + 3P_2 v_2) \right]. \end{aligned} \quad (44)$$

Another set of equations can be derived for the method based on calculation of the $\langle \cos \theta^* \rangle$, Eq. 27. In this case

$$\langle \sin(\Psi_{\text{RP}} - \phi^*) \sin \theta^* \rangle = \frac{\alpha_H}{3} \left[\tilde{A}_0 (P_0 + 2P_2 v_2) - \tilde{A}_2 (P_2 + P_0 v_2) \right], \quad (45)$$

$$\begin{aligned} & \langle \sin(\Psi_{\text{RP}} - \phi^*) \sin \theta^* \cos[2(\phi_H - \phi^*)] \rangle \\ &= \frac{\alpha_H}{3} \left[\tilde{A}_0 (P_2 + P_0 v_2) - \frac{1}{2} \tilde{A}_2 (P_0 + 3P_2 v_2) \right], \end{aligned} \quad (46)$$

where

$$\tilde{A}_0(p_t^H, \eta^H) = \frac{3}{2} \int \frac{d\Omega^*}{4\pi} \frac{d\phi_H}{2\pi} A(\mathbf{p}_H, \mathbf{p}^*) \sin^2 \theta^*, \quad (47)$$

$$\tilde{A}_2(p_t^H, \eta^H) = \frac{3}{2} \int \frac{d\Omega^*}{4\pi} \frac{d\phi_H}{2\pi} A(\mathbf{p}_H, \mathbf{p}^*) \sin^2 \theta^* \cos[2(\phi_H - \phi^*)]. \quad (48)$$

4.6.2. Polarization along the beam direction

For P_z measurement, we consider the average of $\langle \cos \theta_B^* \rangle$ using Eq. 18, where θ_B^* is the polar angle of the daughter baryon in its parent hyperon rest frame, relative to the beam direction.

$$\langle \cos \theta_B^* \rangle = \int \frac{d\Omega^*}{4\pi} A(\mathbf{p}_H, \mathbf{p}^*) (1 + \alpha_H P_z \cos \theta_B^*) \cos \theta_B^* \quad (49)$$

$$= \alpha_H P_z \int \frac{d\Omega^*}{4\pi} A(\mathbf{p}_H, \mathbf{p}^*) \cos^2 \theta_B^*. \quad (50)$$

Thus:

$$P_z = \frac{1}{A_z} \frac{3 \langle \cos \theta_B^* \rangle}{\alpha_H}, \quad (51)$$

where A_z is acceptance correction factor defined as

$$A_z(p_t^H, \eta^H) = 3 \int \frac{d\Omega^*}{4\pi} A(\mathbf{p}_H, \mathbf{p}^*) \cos^2 \theta_B^*. \quad (52)$$

The factor A_z can be determined in a data driven way, similar to the acceptance correction factors in the global polarization measurement, and is typically close to unity.³

4.6.3. Acceptance effects in spin alignment measurements

Spin alignment measurements are significantly more difficult compared to the measurements of the hyperon polarization. The difficulty comes from the fact that while the acceptance effects in the polarization measurements can only change the magnitude of the effect, in the spin alignment measurement the acceptance effects could lead to false spurious signal. We demonstrate this below providing equations for the acceptance correction to the signal for the case of vector mesons experiencing elliptic flow.

One of the main tracking efficiency effects is due to different probabilities if vector meson reconstruction when the daughter particles are emitted along the momentum of the parent particles or perpendicular to that. A toy model study on decay daughters can show that such efficiency effect can be well parameterized by parameter a_2 in the equation

$$A(\phi^*) = A_0(1 + 2a_2(p_T) \cos[2(\phi^* - \phi)]), \quad (53)$$

where ϕ denotes the vector meson azimuthal angle in the laboratory frame.

Then following Eq. 34 and accounting for elliptic flow and efficiency effects, one finds:

$$\begin{aligned} \Delta\rho^{\text{obs}} &\equiv \rho_{00}^{\text{obs}} - \frac{1}{3} = \int \frac{d\Psi_{\text{RP}}}{2\pi} \frac{d\phi^*}{2\pi} \frac{d\phi}{2\pi} (-4/3) \cos[2(\phi^* - \Psi_{\text{RP}})] \\ &\quad \times (1 + 2v_2(p_T) \cos[2(\phi - \Psi_{\text{RP}})])(1 + 2a_2(p_T) \cos[2(\phi^* - \phi)]) \\ &\quad \times (1 - \frac{3}{2} \Delta\rho(p_T) \cos[2(\phi^* - \Psi_{\text{RP}})]) = \Delta\rho - \frac{4}{3} a_2 v_2, \end{aligned} \quad (54)$$

where the superscript “obs” (observed) denotes the value obtained by the direct application of Eq. 34 to the data. One can see that even in the case of “real” $\Delta\rho$ being zero, the observed signal is not zero due to interplay of the elliptic flow and tracking efficiency effects.

Similarly this effect biases the flow measurement as:

$$v_2^{\text{obs}} = v_2 - \frac{3}{4} a_2 \Delta\rho, \quad (55)$$

and the determination of parameter a_2 from data can be done with:

$$a_2^{\text{obs}} = a_2 - \frac{4}{3} v_2 \Delta\rho. \quad (56)$$

The actual values of the spin alignment and elliptic flow can be obtained by solving the above equations Eqs. 54–56 with respect to v_2 , a_2 , and $\Delta\rho$.

The equations above demonstrate only one example of the tracking efficiency effects leading to a spurious spin alignment signal. Another example was discussed in Ref.,⁷⁵ where the authors investigated (and found to be significant) the effect of the finite rapidity acceptance on $\Delta\rho$ measurements.

5. Overview of experimental results

5.1. Global polarization of Λ hyperons

5.1.1. Energy dependence

Global polarization of Λ and $\bar{\Lambda}$ hyperons has been measured in a wide range of collision energies. The first observation of non-zero global polarization was reported in Au+Au collisions at $\sqrt{s_{\text{NN}}} = 7.7\text{--}39$ GeV in the first phase of the beam energy scan program (BES-I) at RHIC by the STAR Collaboration;¹ later it was also confirmed with a better significance at $\sqrt{s_{\text{NN}}} = 200$ GeV.² At the LHC energies the measurements were performed by the ALICE Collaboration.⁷⁶ Figure 5 presents a compilation of the results of the global polarization measurements for Λ and $\bar{\Lambda}$ hyperons at mid-rapidity for mid-central collisions as a function of collision energy. The polarization increases as the collision energy decreases. One would naively expect that the initial orbital angular momentum becomes larger at higher energy,⁴⁹ therefore the polarization would have the same trend, but this argument does not take into account that the initial angular momentum has to be spread over much larger rapidity region and more produced particles, and that the particle production at the midrapidity is almost boost invariant. Another reason for the observed energy dependence might be a dilution effect of the vorticity due to longer lifetime of the system at higher collision energies.

Most of the theoretical calculations rely on the assumptions that (a) the system is in a local thermal equilibrium and (b) that the spin polarization is not modified at later non-equilibrium stages, e.g., by hadronic rescattering.^{77,78} Neither of these assumptions is obvious. Nevertheless, most of the calculations, based on different approaches, such as hydrodynamic models,^{49,79–81} chiral kinetic approach,⁸² and a transport model,⁷⁰ surprisingly well reproduce the observed energy dependence of the global polarization at the quantitative level, as seen in Fig. 5. Note that there still exists a disagreement between the data and models in differential measurements, which we discuss in the following sections. Based on Eq. (2), the vorticity can be estimated as $\omega \approx k_B T (P_\Lambda + P_{\bar{\Lambda}}) / \hbar$ with T being the system temperature at the time of particle emission. The polarization averaged over $\sqrt{s_{\text{NN}}}$ in the BES-I results in $\omega \approx (9 \pm 1) \times 10^{21} \text{ s}^{-1}$, leading to the finding of the most vortical fluid ever observed.¹

From empirical estimates¹⁸ based on the directed flow measurements, see Sec. 2.1, the global polarization signal at the LHC energies is expected to be an order of a few per mill. The results from the ALICE Collaboration are consistent with zero with statistical uncertainties of the order of the expected signal. At lower energies, it is expected that the kinematic vorticity becomes maximum around $\sqrt{s_{\text{NN}}} = 3$ GeV and vanishes at $\sqrt{s_{\text{NN}}} = 2m_N$ (m_N is the nucleon mass) near the threshold of nucleon pair production because the total angular momentum of the system at such energies becomes close to zero.^{85–87} In such high baryon density region, the system would no longer experience a partonic phase but be in a hadronic phase during the

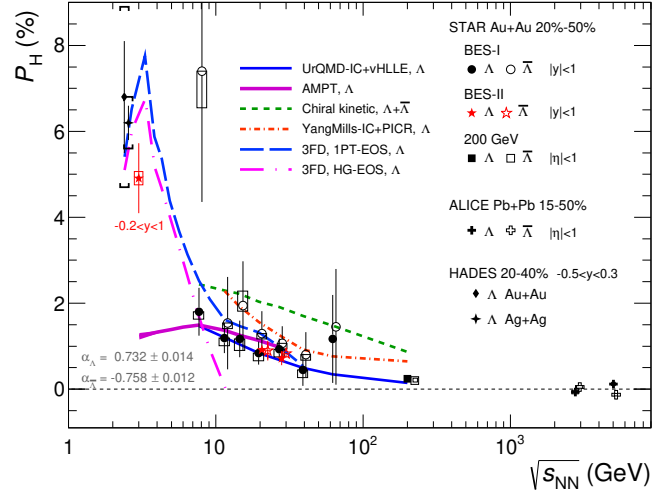


Fig. 5. Collision energy dependence of Λ and $\bar{\Lambda}$ global polarization for mid-central heavy-ion collisions⁸³ compared to various model calculations.^{49, 70, 79, 81, 82} The experimental data from the original publications are rescaled accounting for the recent update of the Λ decay parameters⁸⁴ indicated in the figure.

entire system evolution. Therefore, it would be interesting to check whether the polarization changes smoothly with the beam energy. Recently the STAR Collaboration has reported Λ global polarization in Au+Au collisions at $\sqrt{s_{NN}} = 3$ GeV,⁸³ followed by results on Λ global polarization in Au+Au collisions at $\sqrt{s_{NN}} = 2.4$ GeV and Ag+Ag collisions at $\sqrt{s_{NN}} = 2.55$ GeV by the HADES Collaboration.⁸⁸ The results indicate that the global polarization still increase at these energies, although the current uncertainties may be too large to see the expected trend.

Calculation from the three-fluid dynamics (3FD)⁸¹ incorporating the equation of state (EoS) for the first-order phase transition (1PT) captures the trend of the experimental data. The 3FD model also shows sensitivity of the global polarization to EoS as seen in some difference in the calculations for the first-order phase transition and hadronic (HG) EoS.

5.1.2. Particle-antiparticle difference

As discussed in Sec. 2.2, the initial and/or later-stage magnetic field created in heavy-ion collisions could lead to a difference in the global polarizations of particles and antiparticles. The experimental results, presented in Fig 5, do not show any significant difference in polarizations of Λ and $\bar{\Lambda}$, already indicating that the thermal vorticity, rather than the magnetic field contribution, is the dominant source of the observed global polarization. Figure 6 presents directly the differences in the global polarizations of Λ and $\bar{\Lambda}$ as a function of $\sqrt{s_{NN}}$.⁸⁹ The new RHIC BES-II results from Au+Au collisions at 19.6 GeV and 27 GeV greatly improve the statis-

tical uncertainty in the measurements, and show no significant difference between particle-antiparticle polarizations. Following Eq. 2, one could put an upper limit on the magnetic field effect assuming the local thermodynamic equilibrium for the spin degrees of freedom:

$$\Delta P_H = P_{\bar{\Lambda}} - P_{\Lambda} = \frac{2|\mu_{\Lambda}|B}{T}, \quad (57)$$

where $\mu_{\Lambda} = -\mu_{\bar{\Lambda}} = -0.613\mu_N$ with μ_N being the nuclear magneton. Thus, one arrives at the upper limit on the magnitude of the magnetic field $B \lesssim 10^{13}$ T assuming the temperature $T = 150$ MeV and ignoring the feed-down contributions (see Sec. 4.4). The estimated magnitude of the magnetic field is still considerably large and presents an important input for the dynamical modeling e.g., magneto-hydrodynamics, constraining the electric conductivity of the plasma.

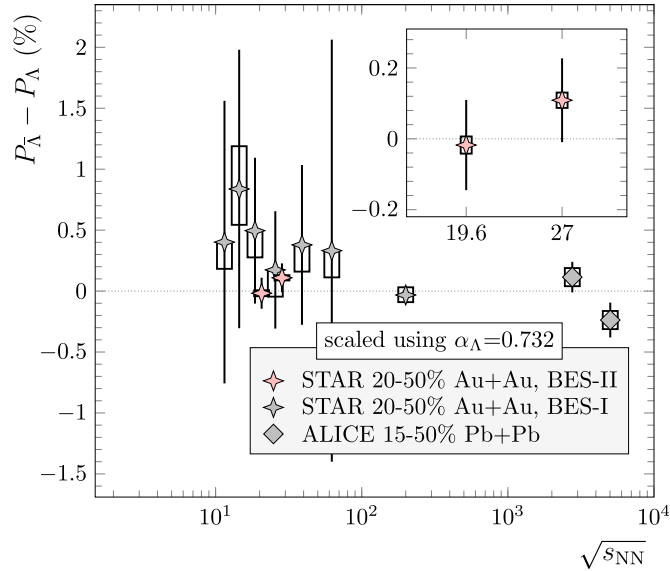


Fig. 6. Collision energy dependence of the difference in global polarizations of $\bar{\Lambda}$ and Λ hyperons, $P_{\bar{\Lambda}} - P_{\Lambda}$. The figure is taken from Ref.⁸⁹

It should be noted that several other sources could contribute to the polarization difference. Ref.⁴⁰ suggests that the different space-time distributions and emission times of Λ and $\bar{\Lambda}$ hyperons lead to the polarization difference. $\bar{\Lambda}$ hyperons, emitted earlier in time, are less affected by the dilution of the vorticity with the system expansion, leading to larger polarization of $\bar{\Lambda}$. On the other hand, Ref.⁹⁰ argues that the formation time of Λ is smaller than that of $\bar{\Lambda}$, leading to larger polarization of Λ . The actual situation might be even more complicated since the spin-orbit coupling may take place at quark level. Ref.⁴¹ reported that the strong interaction

with meson field could make $\bar{\Lambda}$ polarization larger. The effect of chemical potential becomes important at lower energies as it appears in the Fermi-Dirac distribution (see Eq. (6)). Non-zero baryon chemical potential is expected to lead to larger polarization of $\bar{\Lambda}$,⁴² though the effect may be rather small. The feed-down effects with non-zero baryon chemical potential might lead to the opposite relation²³ but it would depend on the relative abundance at different phase space. Having these complications in mind, non-significant difference in the observed global polarization of Λ and $\bar{\Lambda}$, $P_{\bar{\Lambda}} - P_{\Lambda}$, does not exclude a limited contribution from the magnetic field.

5.1.3. Differential measurements

Recently available high statistics data permit to study global polarization differentially, as a function of centrality, transverse momentum, and rapidity. Model calculations show that the initial angular momentum of the system increases from central to mid-central collisions and then decreases in peripheral collisions since the energy density decreases,¹⁰ but the vorticity, hence the global polarization, are expected to increase in more peripheral collisions.⁹¹ Figure 7(left) shows centrality dependence of Λ ($\bar{\Lambda}$) global polarization in Au+Au collisions at $\sqrt{s_{\text{NN}}} = 200$ and 3 GeV,^{2,83} where the increasing trend towards peripheral collisions can be clearly seen. Viscous hydrodynamics models^{79,92} qualitatively describe the centrality dependence of global polarization as shown in the figure.

As already mentioned, the “global” polarization refers to the polarization component along the system orbital angular momentum averaged over all particles and all momenta. The same component (denoted as P_{-y}), but measured for a particular kinematics, can deviate from the global average; in this case the term “local” polarization is more appropriate. For example, the initial velocity shear resulting in the global vorticity would change with rapidity, i.e., the shear might be larger in forward/backward rapidity, also depending on the collision energy.^{91,93} Theoretical models such as hydrodynamics and transport models predict the rapidity dependence differently;^{87,94–97} some models predict that the polarization goes up in forward (backward) rapidity while the others predict decreasing trend in larger rapidities. The hydrodynamic models using different initial conditions and frameworks also predict different trends (see Fig. 7(right)). The first study was performed at $\sqrt{s_{\text{NN}}} = 200$ GeV² as shown in Fig. 7(right) and no significant rapidity dependence was observed, which may be expected at high collision energy as the shear should be weaker at midrapidity because of longitudinally boost invariance. Recent measurement at $\sqrt{s_{\text{NN}}} = 3$ GeV from STAR⁸³ also found no strong rapidity dependence within $-0.2 < y < 1$, even at the rapidity close to the beam rapidity ($y_{\text{beam}} = 1.02$ at $\sqrt{s_{\text{NN}}} = 3$ GeV). Similarly, no dependence on rapidity is observed at $\sqrt{s_{\text{NN}}} = 2.55$ GeV by the HADES experiment.⁸⁸ The uncertainties of the data are still large and this question should be further studied in future analyses with better statistics and upgraded/new detectors.

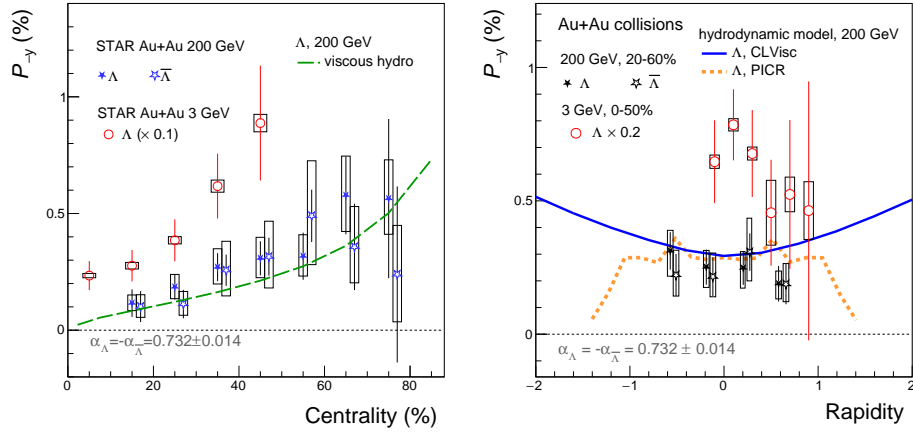


Fig. 7. (Left) Centrality dependence of $\Lambda(\bar{\Lambda})$ of P_{-y} polarization component in Au+Au collisions at $\sqrt{s_{NN}} = 3$, and 200 GeV compared to viscous hydrodynamic model calculation.⁹² (Right) Rapidity dependence of $\Lambda(\bar{\Lambda})$ P_{-y} compared to Particle-in-Cell Relativistic (PICR) hydrodynamics model⁹⁶ and viscous hydrodynamic model CLVisc.⁹⁵ Note that the data for 3 GeV in the left (right) plot are scaled by 0.1 (0.2), and the average pseudorapidity for 200 GeV is converted to the rapidity in the right panel.

It should be noted that the polarization P_{-y} component seems to have little dependence on the hyperon transverse momentum p_T ,^{2,83,88,89} which qualitatively agrees with theoretical models that predict a mild p_T dependence. Figure 8(left) shows hyperons' transverse momentum dependence of the polarization along the system angular momentum in Au+Au collisions at $\sqrt{s_{NN}} = 200$ GeV, compared to hydrodynamic model calculations with two different initial conditions:²³ Monte Carlo Glauber with the initial source tilt and UrQMD initial state. The UrQMD initial condition includes the initial flow from a preequilibrium phase that would affect the initial velocity field. Similar trend was also seen at lower collision energies.^{83,88,89}

The STAR Collaboration also studied charge asymmetry (A_{ch}) dependence of the global polarization for a possible relation to anomalous chiral effects.³⁸ According to Ref.,⁹⁸ the global polarization could be explained by axial charge separation due to the chiral vortical effect. In addition, the axial current \mathbf{J}_5 can be generated in the system with nonzero vector chemical potential μ_v under a strong magnetic field \mathbf{B} ($\mathbf{J}_5 \propto Qe\mu_v\mathbf{B}$), aka chiral separation effect, where Qe represents net electric charge of particles. For massless quarks, their momentum direction is aligned (anti-aligned) with spin direction for right-handed (left-handed) quarks. Thus the \mathbf{J}_5 , if generated, might contribute to the hyperon global polarization. The event charge asymmetry defined as $A_{ch} = (N_+ - N_-)/(N_+ + N_-)$ where N_+ (N_-) is the number of positively (negatively) charged particles was used to study the possible relation with the polarization assuming $A_{ch} \propto \mu_v$. Figure 8(right) shows Λ and $\bar{\Lambda}$

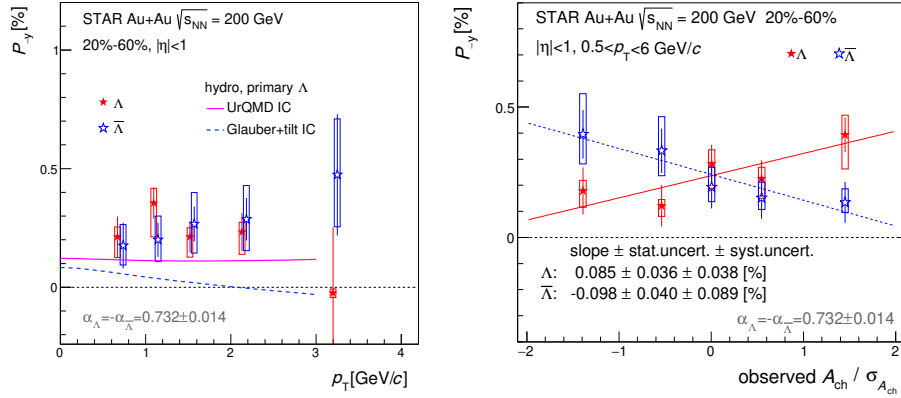


Fig. 8. P_{-y} polarization component of Λ and $\bar{\Lambda}$ as a function of (left) transverse momentum dependence and (right) charge asymmetry A_{ch} normalized with its RMS in Au+Au collisions at $\sqrt{s_{NN}} = 200$ GeV. The figures are adapted from Ref.²

global polarization as a function of A_{ch} for mid-central Au+Au collisions at $\sqrt{s_{NN}} = 200$ GeV. There seems a slight dependence on A_{ch} and the slopes look different for Λ and $\bar{\Lambda}$, although the effect is only at $\sim 2\sigma$ level. The effect of the chemical potential may be an alternative explanation of the difference if the charge asymmetry is correlated with the baryon number asymmetry.^{42,99}

Azimuthal angle dependence of the polarization is also of great interest and has been the subject of debate. The experimental preliminary result from STAR¹⁰⁰ shows larger polarization for hyperons emitted in the in-plane direction than those in out-of-plane direction as shown in Fig. 9, while hydrodynamic and transport models predict it oppositely, i.e., larger polarization in out-of-plane direction.^{26,79,94,101} Based on Glauber simulation shown in Fig. 2(b), one expects $\omega_J (\propto dv_z/dx)$ to be larger in in-plane direction (x -direction in the plot), which is consistent with experimental results. As shown in Fig. 9, the calculation including only the contribution from the kinematic vorticity leads to the opposite sign, while the inclusion of the shear term leads to the correct sign. We discuss this question further in Sec. 5.4 together with the results on polarization along the beam direction in relation to the so-called “spin sign crisis”.

5.2. Global polarization of multi-strange hyperons

Based on the picture of the rotating system, any non-zero spin particles should be polarized in a similar way, along the direction of the initial orbital angular momentum. According to Eq. (2), the magnitude of the polarization depends on the spin of particles. Thus, it is of great interest to study the polarization of different particles with different spin. The STAR Collaboration reported global polarization

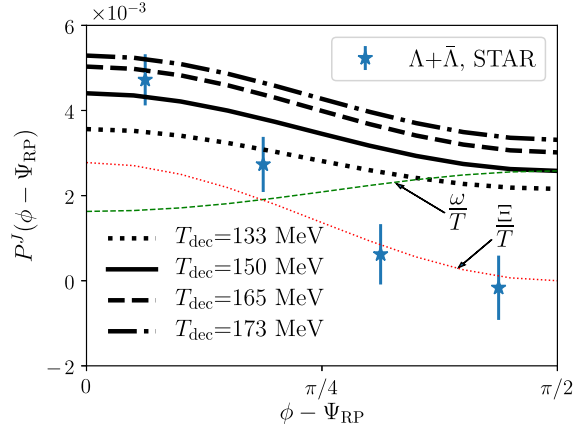


Fig. 9. Polarization of Λ and $\bar{\Lambda}$ hyperons along the initial angular momentum $P_J = P_{-y}$ as a function of hyperons' azimuthal angle relative to the second-order event plane Ψ_2 in 20-50% Au+Au collisions at $\sqrt{s_{NN}} = 200$ GeV (preliminary result from STAR¹⁰⁰), comparing to the hydrodynamic model (vHLLC for 20-60% Au+Au collisions)¹⁰² where T_{dec} is a decoupling temperature assuming the isothermal freeze-out. This figure is taken from Ref.¹⁰²

of Ξ^- ($\bar{\Xi}^+$) and Ω^- ($\bar{\Omega}^+$) hyperons in 200 GeV Au+Au collisions, see Fig. 10. Two independent methods (see Sec. 4.1.1) were used to measure Ξ^- ($\bar{\Xi}^+$) polarization and the results combining Ξ^- and $\bar{\Xi}^+$, and averaging over the two methods is found to be positive at the 2σ level ($\langle P_{\Xi} \rangle = 0.47 \pm 0.10(\text{stat}) \pm 0.23(\text{syst})\%$ for 20-80% centrality), supporting the global vorticity picture. The cascade polarization is measured to be slightly larger than that of inclusive Λ , but the significance of that is below 1σ . The results on Ω^- global polarization hint even larger polarization indicating a possible hierarchy of $P_{\Omega} > P_{\Xi} > P_{\Lambda}$ but with large uncertainties. Based on Eq. (2), the following relation: $P_{\Lambda} = P_{\Xi^-} = \frac{3}{5}P_{\Omega^-}$ is expected. Recent model study shows that this relation is valid only for primary particles, while it leads to $P_{\Lambda} < P_{\Xi^-} < P_{\Omega^-}$ after taking into account the feed-down contribution,⁷² which seems to be consistent with the data. More precise measurements are needed to clarify the particle/spin dependence of the global polarization.

It is worth mentioning that Ω^- hyperon has larger magnetic moment ($\mu_{\Omega^-} = -2.02\mu_N$) compared to those for Λ ($\mu_{\Lambda} = -0.613\mu_N$) and Ξ^- ($\mu_{\Xi^-} = -0.65\mu_N$). Therefore, the polarization difference between Ω^- and $\bar{\Omega}^+$, if any, should be more sensitive to the magnetic field created in the collisions. Another thing to be mentioned is that one of the decay parameter γ_{Ω} is unknown, but expected to be close to either +1 or -1 (see Sec. 4.1.1). Assuming the vorticity picture, one can determine the sign of γ_{Ω} . Currently the experimental result on Ω global polarization has large uncertainty but future high statistics data will allow to resolve the ambiguity.

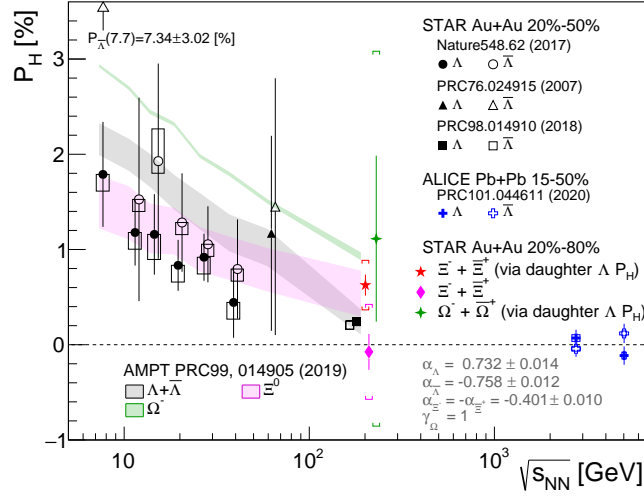


Fig. 10. Global polarization of Ξ and Ω hyperons compared to that of Λ ($\bar{\Lambda}$) as well as transport model calculations. The figure is taken from Ref.¹⁰³

5.3. Global spin alignment of vector mesons

The vorticity should also lead to the global polarization of the vector mesons, such as K^{*0} and ϕ , revealing itself via global spin alignment.^{9,12} The first measurement of the spin alignment was made by the STAR Collaboration at RHIC using 200 GeV Au+Au collisions in 2008¹⁰⁴ but there was no clear signal taking into account the uncertainties of the measurement. More recently, the ALICE and STAR Collaborations reported finite signals,^{105,106} i.e., deviation of ρ_{00} from $1/3$. Figure 11 shows ρ_{00} of K^{*0} and ϕ mesons as a function of collision centrality in a form of the number of participants from MC Glauber simulation, in Pb+Pb collisions at $\sqrt{s_{NN}} = 2.76$ TeV. At lower p_T , the results for both K^{*0} and ϕ mesons indicate $\rho_{00} < 1/3$. The STAR results on ϕ -meson ρ_{00} show large positive deviation from $1/3$ ($\rho_{00} > 1/3$) for $p_T > 1.2$ GeV/c at lower collision energies, while results on K^{*0} are consistent with zero as shown in Fig. 12. The dependence of ϕ -meson spin alignment signal on transverse momentum and centrality is not systematic; the signal seems to change sign and become negative at higher transverse momenta as well as in more central collisions, At present the dependence on transverse momentum and centrality can not be explained in any scenario.

Note that in the vorticity scenario, the spin alignments signal is expected to be very small $\Delta\rho \approx (\omega/T)^2/3 \approx 4P_H^2/3$. Taking into account the hyperon global polarization measurements presented in Fig. 5, the spin alignment signal should be of the order of 10^{-5} at the top RHIC energy and of the order of 10^{-3} at lowest BES energy, which is too small to explain the reported large deviation. If the vector mesons are produced via quark coalescence, ρ_{00} of vector mesons can be expressed

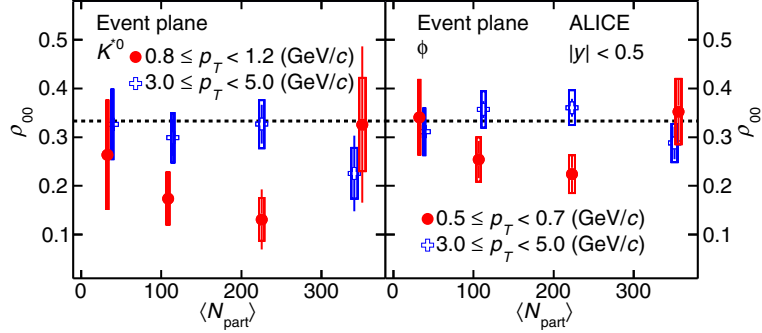


Fig. 11. Global spin alignment of K^{*0} and ϕ mesons shown as the spin density matrix element ρ_{00} with quantization axis chosen along the system orbital angular momentum measured in Pb+Pb collisions at $\sqrt{s_{NN}}=2.76$ TeV by the ALICE Collaboration. The figure is taken from Ref.¹⁰⁵

via the quark (antiquark) polarization $P_q(P_{\bar{q}})$ as $\rho_{00} = (1 - P_q P_{\bar{q}})/(3 + P_q P_{\bar{q}}) \approx (1 - 4P_q P_{\bar{q}}/3)/3$.¹² If $P_q = P_{\bar{q}} = \omega/(2T)$, $\rho_{00} \approx [1 - (\omega/T)^2/3]/3$ which is consistent with the thermal approach.²³ If the particle production for the p_T of interest is dominated by fragmentation process, the ρ_{00} approximates $\rho_{00} \approx (1 + 4P_q^2/3)/3$ leading to $\rho_{00} > 1/3$, but the deviation is again expected to be very small.¹² The only possibility to have large signal in the vorticity based scenario could arise if the vorticity fluctuations are much larger than its average. Note that spin alignment signal is proportional to the (mean root) square of vorticity, while the hyperon polarization is proportional to its average.

References^{108,109} suggest that the mean field of ϕ -mesons could play a role in ϕ ρ_{00} but not in K^{*0} ρ_{00} because of mixing of different flavors. The model involving the strong force seems to explain the energy dependence of ϕ ρ_{00} as shown with the solid line in Fig. 12. Note that in the given p_T range the ϕ ρ_{00} at the LHC is consistent with zero.

Charm quarks are produced via hard scattering of partons at the collision, with a time scale of $\tau \sim 1/(2m_{HQ}) \sim 0.1$ fm/c. Therefore, one may expect larger effect of the initial magnetic field as well as vorticity on the polarization of J/ψ which consists of charm and anti-charm quarks. The ALICE Collaboration reported inclusive J/ψ polarization relative to the event plane in Pb+Pb collisions at $\sqrt{s_{NN}} = 5.02$ TeV at forward rapidity ($2.5 < y < 4$).¹¹⁰ Figure 13 shows J/ψ polarization parameter λ_θ (see Eq. 36) as a function of centrality. Non-zero λ_θ means finite polarization of J/ψ . The observed signal of $0.1 < \lambda_\theta < 0.2$ corresponds to $0.29 > \rho_{00} > 0.25$, a large negative deviation from $1/3$ and opposite to that of ϕ -mesons. This measurement was performed at forward rapidity ($2.5 < y < 4$) and the measurements at mid-rapidity both at the LHC and RHIC¹¹¹ energies are needed for a better understanding of the phenomena. The regeneration mechanism of the J/ψ production that becomes significant at the LHC energies, especially at low p_T , might also complicate the interpretation of the data.

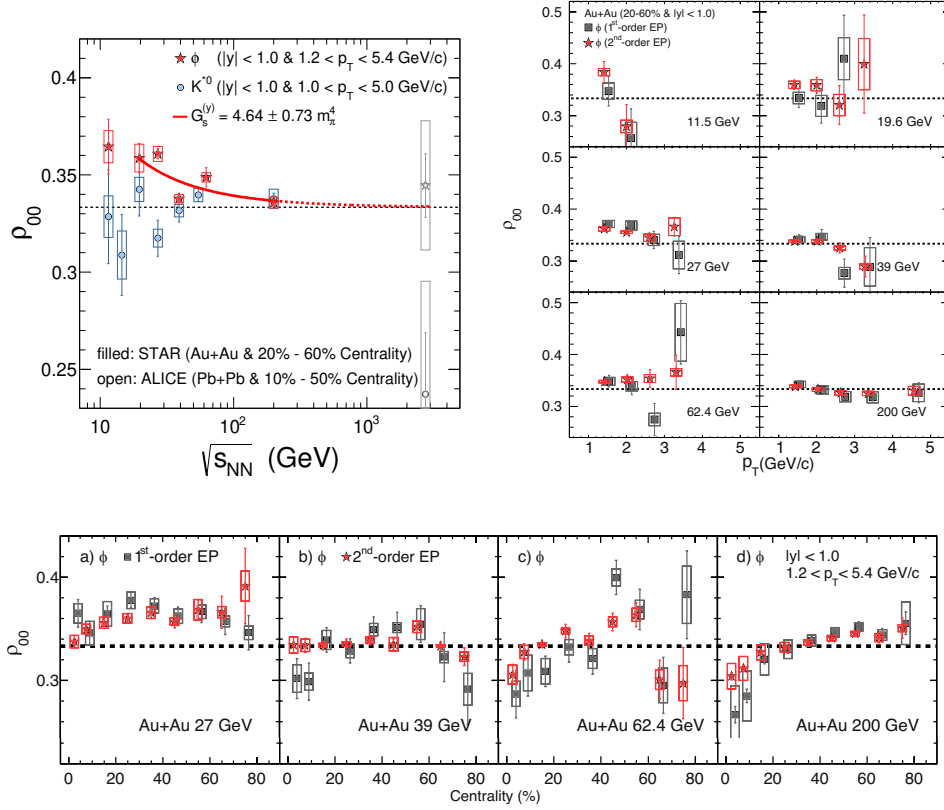


Fig. 12. K^{*0} and ϕ mesons spin density matrix element with quantization axis along the system orbital angular momentum in Au+Au collisions by the STAR experiment. The results are shown as a function of collision energy $\sqrt{s_{NN}}$, transverse momentum, and centrality. The figures are taken from Ref.¹⁰⁷

Obviously the spin alignment measurements still need further investigations, both theoretically and experimentally. These are difficult measurements, and as discussed in Sec. 4.5 and 4.6.3 strongly dependent on complete understanding of the tracking and acceptance effects. Future analyses, in particular based on new high statistics data will allow us to study the spin alignment in much more detail including other particles such as charged $D^{*112,113}$ and Υ .¹¹⁴

5.4. Polarization along the beam direction

As discussed in Sec. 2.3, anisotropic transverse flow leads to nonzero vorticity component along the beam direction, with the direction of vorticity changing with the azimuthal angle,^{18,19} as depicted by open arrows in Fig. 3(left). The polarization along the beam direction P_z was first measured with Λ hyperons by the STAR Collaboration at RHIC.³ Later, it was also observed by the ALICE Collaboration

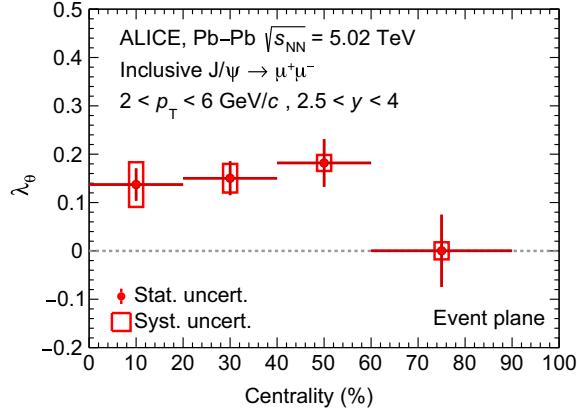


Fig. 13. Spin alignment of inclusive J/ψ along the system orbital angular momentum in Pb+Pb collisions at $\sqrt{s_{NN}} = 5.02$ TeV from ALICE Collaboration.¹¹⁰ The measurement was performed within $2.5 < y < 4$ and $2 < p_T < 6$ GeV/c.

at the LHC energy.¹¹⁵ As expected from the elliptic flow picture, P_z exhibits a quadrupole or $\sin(2\phi)$ pattern as shown in Fig. 14(left). The polarization is quantified by a second-order Fourier sine coefficient and studied as a function of centrality, see Fig. 15. The results show a clear centrality dependence similar to that of elliptic flow except in most peripheral collisions. The polarization magnitudes at RHIC and the LHC are rather similar, indicating weak collision energy dependence unlike in the global polarization case.

It was found that hydrodynamic and transport models that successfully reproduce the energy dependence of the global polarization fail badly in predictions of the magnitude and the sign (phase) of the azimuthal angle modulation differently.^{3, 19, 20, 95, 96, 101, 117, 118} This was true for several hydrodynamics models using different approaches and initial conditions. The chiral kinetic approach accounting for the nonequilibrium effects of the spin degrees of freedom gives the correct sign of the P_z modulation.¹¹⁸ Interestingly, the Blast-Wave model which is a simplified model of hydrodynamics with a few freeze-out parameters⁴⁵ (taken from STAR publication in 2005!) describes the data very well.³

More recently, two independent groups pointed out that accounting for contribution from the fluid velocity shear (see Sec. 3.2) might help to explain the disagreement between the data and theoretical calculations. As shown in Fig. 14(left), the contribution from the kinematic shear, as that in the hydrodynamic model,¹⁰² exhibits an opposite sign in P_z modulation to that of the kinematic vorticity, and as a consequence, combining the two effects leads to a trend similar to the data if additionally the model assumes the isothermal freeze-out. Hydrodynamic model (MUSIC with AMPT initial conditions) including the shear contribution,¹¹⁹ and assuming that Λ inherits the polarization from the strange quark, can also qualitatively describe the measurements including the centrality dependence as shown

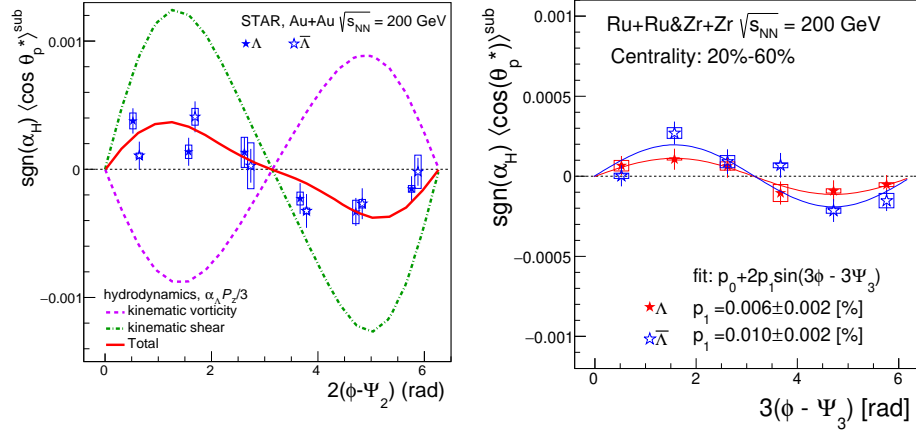


Fig. 14. (Left) Raw signal of polarization along the beam direction, $\langle \cos \theta_p^* \rangle$, of Λ and $\bar{\Lambda}$ hyperons as a function of azimuthal angle relative to the second-order event plane in Au+Au collisions at $\sqrt{s_{\text{NN}}} = 200$ GeV.³ Hydrodynamic model calculations including kinematic vorticity and kinematic shear separately, as well as the sum of the two are shown by lines.¹⁰² (Right) Same as left figure for polarization relative to the third-order event plane in R+Ru and Zr+Zr collisions at $\sqrt{s_{\text{NN}}} = 200$ GeV.¹¹⁶

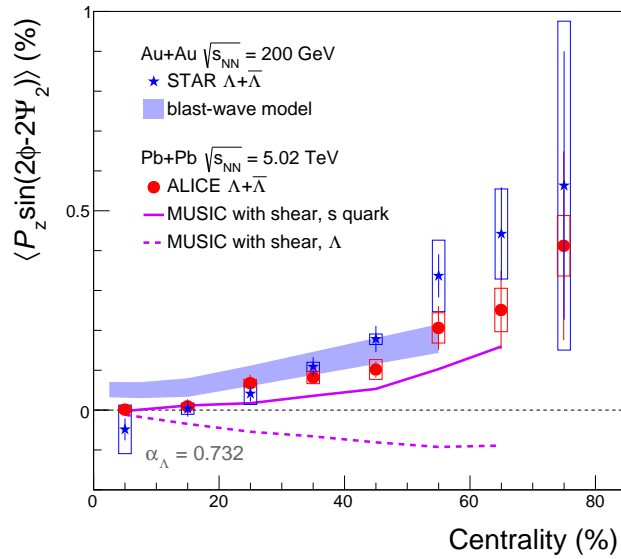


Fig. 15. The second-order sine modulation of Λ polarization along the beam direction as a function of centrality at RHIC³ and the LHC¹¹⁵ compared to various model calculations.^{3,119} The experimental data are rescaled with Λ decay parameter $\alpha_{\Lambda} = 0.732$.⁸⁴

in Fig. 15. But the predictions change to the opposite sign if the polarization is calculated using Λ mass. It should be noted that the thermal vorticity and shear contributions are largely canceled out^{120–123} and the final result depends strongly on the detailed implementation of those contributions. Thus the spin sign puzzle still needs more investigations.

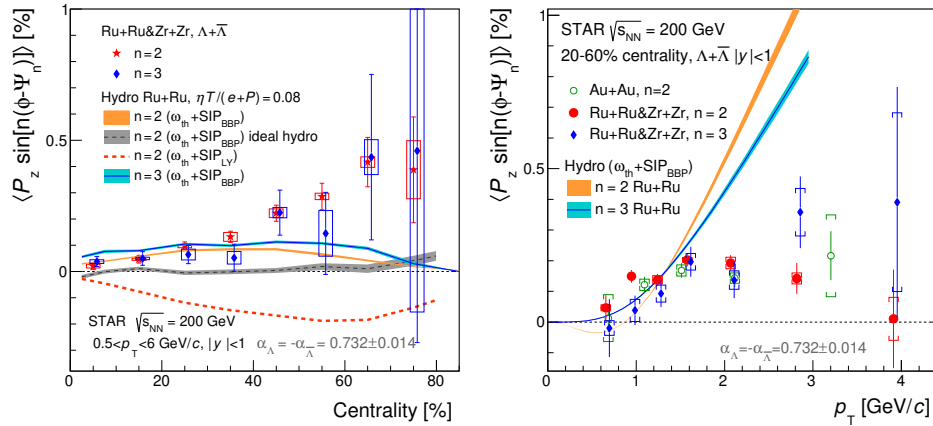


Fig. 16. The second and third-order sine modulation of Λ polarization along the beam direction as a function of centrality (left) and hyperons' transverse momentum (right) in Ru+Ru and Zr+Zr collisions at $\sqrt{s_{NN}} = 200$ GeV.¹¹⁶ Solid and dashed lines are the calculations from hydrodynamic model with particular implementation of the shear induced polarization (SIP).¹²³ See texts for the detail.

As predicted in Ref.,¹⁸ higher harmonic anisotropic flow should also lead to a similar vorticity structure and polarization along the beam direction. Recently, the STAR Collaboration has reported Λ polarization along the beam direction relative to the third harmonic event plane in isobar Ru+Ru and Zr+Zr collisions $\sqrt{s_{NN}} = 200$ GeV;¹¹⁶ these results are shown in Fig. 14(right). The sine modulation of P_z relative to the third-order event plane was observed similarly to the second-order case, indicating a sextupole pattern of vorticity induced by triangular flow as depicted in Fig. 3(right).

Figure 16(left) shows P_z sine coefficients relative to the second and third order harmonic event planes as a function of centrality in the isobar collisions. The third-order result seems to increase towards peripheral collisions as the second-order does. Calculations from hydrodynamic model with two different implementations of the shear induced polarization (SIP), based on Ref.⁵¹ by Becattini-Buzzegoli-Palermo (BBP) and on Ref.⁵⁰ by Liu-Yin (LY), are also compared. The calculations with “SIP_{BBP}” reasonably well describe the data for both the second and third-orders except peripheral collisions. The calculation with “SIP_{LY}” leads to the opposite sign to the data but note that it provides the correct sign if the mass of strange

quark is used instead of Λ mass as shown in Fig. 15. It is also worth to mention that the calculation with a nearly zero specific shear viscosity (denoted as “ideal hydro”) leads to almost zero P_z sine coefficient, which indicates that the P_z measurement could provide an additional constraint on the shear viscosity of the medium. Figure 16(right) shows p_T dependence of the second and third-order P_z sine coefficients. The third-order result is found to be comparable in magnitude to the second-order result, slightly smaller at low p_T and showing a hint of overpassing the second-order at high p_T . This trend is similar to what was observed in p_T dependence of the elliptic and triangular flow,¹²⁴ which further supports the picture of anisotropic-flow-driven polarization. The model incorporating the shear induced polarization of SIP_{BBP} is comparable to the data at low p_T but not the p_T dependence in detail.

6. Open questions and future perspective

Summarizing the discussion in Sec. 5, one tend to conclude that while the theoretical description of the global polarization, including its energy dependence, is rather good, our understanding of the local polarization measurements, in particular the azimuthal angle dependence of the polarization along the beam direction is far from satisfactory. Surprisingly, the data is much better described by “naive” Blast-Wave model including only nonrelativistic vorticity, than by more sophisticated hydrodynamical calculations (including contribution from temperature gradients and acceleration), which very often differ from the data at the qualitative level. Recent calculations including the shear induced polarization make the comparison somewhat better, but still unsatisfactory. The disagreements with theoretical models definitely need further investigation in future, including the role of different freeze-out scenarios, validity of Cooper-Frye prescription, relative contributions of kinematic vorticity, acceleration, SIP, SHE, and temperature gradients. Comparison of more advanced calculations with new measurements should be also able to provide information of vorticity evolution and spin equilibration relaxation times.

From experimental point of view, in the next few years several new precise measurements will be performed to shed more light on the topics of interest, such as particle-antiparticle polarization splitting, rapidity and azimuthal angle dependencies, and particle species dependence. Below we list possible near-future measurements intended to provide more information on the vorticity and polarization phenomena in heavy-ion collisions.

- Polarization splitting between particles and antiparticles, including particles with larger magnitude of the magnetic moment such as Ω . It will further constrain the magnetic field time evolution and its strength at freeze-out, and the electric conductivity of quark-gluon plasma.
- Precise measurements of multistrange hyperon polarization to study particle species dependence and confirm the vorticity-based picture of polarization. Measurement with Ω will also constrain unknown decay parameter

- $\gamma\Omega$.
- Precise differential measurements of the azimuthal angle and rapidity dependence of P_J (P_{-y}).
- Detailed measurement of P_z induced by elliptic and higher harmonic flow. In particular this study could help to identify the contribution from SIP, which is expected to be different for different harmonics.
- Application of the event-shape-engineering technique¹²⁵ testing the relationship between anisotropic flow and polarization.
- Measuring P_x to complete all the components of polarization and compare the data to the Glauber estimates and full hydrodynamical calculations.
- Circular polarization P_ϕ to search for toroidal vortex structures
- The particle-antiparticle difference in the polarization dependence on azimuthal angle at lower collision energies testing the Spin-Hall Effect.
- Understanding of the vector meson spin alignment measurements including new results with corrections of different detector effects.
- Measurement of the hyperon polarization correlations to access the scale of vorticity fluctuations.
- Measurement of the hyperon polarization in pp collisions to establish/disprove possible relation to the single spin asymmetry effect.

7. Summary

The polarization phenomena in heavy-ion collisions appeared to be an extremely interesting and important subject overarching such questions as the nature of the spin and spin structure of the hadrons, evolution of the QGP and its hadronization, and finally the freeze-out of the system. While many, or better to say, most of the details of the entire picture is far from being even well formulated, it is clear that following this direction we might expect many important discoveries.

The observed global polarization of hyperons in heavy-ion collisions is found to be well described by hydrodynamic and microscopic transport models based on the local vorticity of the fluid averaged over the freeze-out hypersurface under assumption of the local thermal equilibrium of the spin degrees of freedom. Furthermore, the measurement of hyperon polarization along the beam direction confirmed the local vorticity induced by anisotropic collective flow, adding to the evidences of ideal fluid dynamics of the quark-gluon plasma. These measurements opened new direction to study the dynamics of quark-gluon plasma and spin transport in the hot and dense medium, triggering a lot of theoretical interest on spin dynamics in general. Despite the successful description of the average global polarization, when looking into the detailed comparison between the data and models in differential measurements, there are still many open questions to be solved. The spin alignment measurements of vector mesons are very intriguing, but far from satisfactory understanding. More precise measurements with different particle species and a wider detector acceptance that will be available in near future at RHIC and the LHC

and future experiments at new facilities will be extremely helpful to shed light on existing issues.

Acknowledgments

The discussions with F. Becattini, and C. Shen are gratefully acknowledged.

S. Voloshin is supported by the U.S. Department of Energy Office of Science, Office of Nuclear Physics under Award No. DE-FG02-92ER40713. T. Niida is supported by JSPS KAKENHI Grant Number JP22K03648.

References

1. **STAR** Collaboration, L. Adamczyk *et al.*, “Global Λ hyperon polarization in nuclear collisions: evidence for the most vortical fluid”, *Nature* **548**, 62–65 (2017), [arXiv:1701.06657](#).
2. **STAR** Collaboration, J. Adam *et al.*, “Global polarization of Λ hyperons in Au+Au collisions at $\sqrt{s_{NN}} = 200$ GeV”, *Phys. Rev. C* **98**, 014910 (2018), [arXiv:1805.04400](#).
3. **STAR** Collaboration, J. Adam *et al.*, “Polarization of Λ ($\bar{\Lambda}$) hyperons along the beam direction in Au+Au collisions at $\sqrt{s_{NN}} = 200$ GeV”, *Phys. Rev. Lett.* **123**, no. 13, 132301 (2019), [arXiv:1905.11917](#).
4. **STAR** Collaboration, K. H. Ackermann *et al.*, “Elliptic flow in Au + Au collisions at $\sqrt{s_{NN}} = 130$ GeV”, *Phys. Rev. Lett.* **86**, 402–407 (2001), [arXiv:nucl-ex/0009011](#).
5. **STAR** Collaboration, C. Adler *et al.*, “Disappearance of back-to-back high p_T hadron correlations in central Au+Au collisions at $\sqrt{s_{NN}} = 200$ GeV”, *Phys. Rev. Lett.* **90**, 082302 (2003), [arXiv:nucl-ex/0210033](#).
6. **PHENIX** Collaboration, S. S. Adler *et al.*, “Suppressed π^0 production at large transverse momentum in central Au+ Au collisions at $\sqrt{s_{NN}} = 200$ GeV”, *Phys. Rev. Lett.* **91**, 072301 (2003), [arXiv:nucl-ex/0304022](#).
7. S. A. Voloshin, A. M. Poskanzer, and R. Snellings, “Collective phenomena in non-central nuclear collisions”, *Landolt-Bornstein* **23**, 293–333 (2010).
8. Z.-T. Liang and X.-N. Wang, “Globally polarized quark-gluon plasma in non-central A+A collisions”, *Phys. Rev. Lett.* **94**, 102301 (2005). [Erratum: *Phys.Rev.Lett.* 96, 039901 (2006)].
9. S. A. Voloshin, “Polarized secondary particles in unpolarized high energy hadron-hadron collisions?”, [arXiv:nucl-th/0410089](#).
10. F. Becattini, F. Piccinini, and J. Rizzo, “Angular momentum conservation in heavy ion collisions at very high energy”, *Phys. Rev. C* **77**, 024906 (2008), [arXiv:0711.1253](#).
11. S. B. Nurushev, M. F. Runtso, and M. N. Strikhanov, *Introduction to polarization physics*. Springer Berlin, Heidelberg, 2013.
12. Z.-T. Liang and X.-N. Wang, “Spin alignment of vector mesons in non-central A+A collisions”, *Phys. Lett. B* **629**, 20–26 (2005), [arXiv:nucl-th/0411101](#).
13. **STAR** Collaboration, B. I. Abelev *et al.*, “Global polarization measurement in Au+Au collisions”, *Phys. Rev. C* **76**, 024915 (2007), [arXiv:0705.1691](#). [Erratum: *Phys.Rev.C* 95, 039906 (2017)].
14. J.-H. Gao, S.-W. Chen, W.-t. Deng, Z.-T. Liang, Q. Wang, and X.-N. Wang, “Global quark polarization in non-central A+A collisions”, *Phys. Rev. C* **77**, 044902 (2008), [arXiv:0710.2943](#).

15. B. Betz, M. Gyulassy, and G. Torrieri, “Polarization probes of vorticity in heavy ion collisions”, *Phys. Rev. C* **76**, 044901 (2007).
16. W. M. Serenone, J. a. G. P. Barbon, D. D. Chinellato, M. A. Lisa, C. Shen, J. Takahashi, and G. Torrieri, “A polarization from thermalized jet energy”, *Phys. Lett. B* **820**, 136500 (2021), [arXiv:2102.11919](#).
17. L.-G. Pang, H. Petersen, Q. Wang, and X.-N. Wang, “Vortical Fluid and Λ Spin Correlations in High-Energy Heavy-Ion Collisions”, *Phys. Rev. Lett.* **117**, no. 19, 192301 (2016), [arXiv:1605.04024](#).
18. S. A. Voloshin, “Vorticity and particle polarization in heavy ion collisions (experimental perspective)”, *EPJ Web Conf.* **171**, 07002 (2018), [arXiv:1710.08934](#).
19. F. Becattini and Iu. Karpenko, “Collective longitudinal polarization in relativistic heavy-ion collisions at very high energy”, *Phys. Rev. Lett.* **120**, 012302 (2018), [arXiv:1707.07984](#).
20. X.-L. Xia, H. Li, Z.-B. Tang, and Q. Wang, “Probing vorticity structure in heavy-ion collisions by local Λ polarization”, *Phys. Rev. C* **98**, 024905 (2018), [arXiv:1803.00867](#).
21. F. Becattini and F. Piccinini, “The Ideal relativistic spinning gas: Polarization and spectra”, *Annals Phys.* **323**, 2452–2473 (2008), [arXiv:0710.5694](#).
22. F. Becattini, V. Chandra, L. Del Zanna, and E. Grossi, “Relativistic distribution function for particles with spin at local thermodynamical equilibrium”, *Annals Phys.* **338**, 32–49 (2013), [arXiv:1303.3431](#).
23. F. Becattini, I. Karpenko, M. Lisa, I. Upsal, and S. Voloshin, “Global hyperon polarization at local thermodynamic equilibrium with vorticity, magnetic field and feed-down”, *Phys. Rev. C* **95**, no. 5, 054902 (2017), [arXiv:1610.02506](#).
24. L. P. Csernai, V. K. Magas, and D. J. Wang, “Flow Vorticity in Peripheral High Energy Heavy Ion Collisions”, *Phys. Rev. C* **87**, no. 3, 034906 (2013), [arXiv:1302.5310](#).
25. P. Bożek and I. Wyskiel, “Directed flow in ultrarelativistic heavy-ion collisions”, *Phys. Rev. C* **81**, 054902 (2010).
26. F. Becattini, G. Inghirami, V. Rolando, A. Beraudo, L. Del Zanna, A. De Pace, M. Nardi, G. Pagliara, and V. Chandra, “A study of vorticity formation in high energy nuclear collisions”, *Eur. Phys. J. C* **75**, no. 9, 406 (2015), [arXiv:1501.04468](#). [Erratum: *Eur.Phys.J.C* 78, 354 (2018)].
27. **STAR** Collaboration, L. Adamczyk *et al.*, “Beam-Energy Dependence of the Directed Flow of Protons, Antiprotons, and Pions in Au+Au Collisions”, *Phys. Rev. Lett.* **112**, no. 16, 162301 (2014), [arXiv:1401.3043](#).
28. S. Singha, P. Shanmuganathan, and D. Keane, “The first moment of azimuthal anisotropy in nuclear collisions from AGS to LHC energies”, *Adv. High Energy Phys.* **2016**, 2836989 (2016), [arXiv:1610.00646](#).
29. **ALICE** Collaboration, B. Abelev *et al.*, “Directed Flow of Charged Particles at Midrapidity Relative to the Spectator Plane in Pb-Pb Collisions at $\sqrt{s_{NN}} = 2.76$ TeV”, *Phys. Rev. Lett.* **111**, no. 23, 232302 (2013), [arXiv:1306.4145](#).
30. **STAR** Collaboration, B. I. Abelev *et al.*, “System-size independence of directed flow at the Relativistic Heavy-Ion Collider”, *Phys. Rev. Lett.* **101**, 252301 (2008), [arXiv:0807.1518](#).
31. **ALICE** Collaboration, S. Acharya *et al.*, “Probing the effects of strong electromagnetic fields with charge-dependent directed flow in Pb-Pb collisions at the LHC”, *Phys. Rev. Lett.* **125**, no. 2, 022301 (2020), [arXiv:1910.14406](#).
32. **STAR** Collaboration, L. Adamczyk *et al.*, “Azimuthal anisotropy in Cu+Au

- collisions at $\sqrt{s_{NN}} = 200$ GeV”, *Phys. Rev. C* **98**, no. 1, 014915 (2018), [arXiv:1712.01332](#).
33. D. E. Kharzeev, L. D. McLerran, and H. J. Warringa, “The Effects of topological charge change in heavy ion collisions: ‘Event by event P and CP violation’”, *Nucl. Phys. A* **803**, 227–253 (2008), [arXiv:0711.0950](#).
 34. V. Skokov, A. Y. Illarionov, and V. Toneev, “Estimate of the magnetic field strength in heavy-ion collisions”, *Int. J. Mod. Phys. A* **24**, 5925–5932 (2009), [arXiv:0907.1396](#).
 35. V. Voronyuk, V. D. Toneev, W. Cassing, E. L. Bratkovskaya, V. P. Konchakovski, and S. A. Voloshin, “(Electro-)Magnetic field evolution in relativistic heavy-ion collisions”, *Phys. Rev. C* **83**, 054911 (2011), [arXiv:1103.4239](#).
 36. K. Tuchin, “Particle production in strong electromagnetic fields in relativistic heavy-ion collisions”, *Adv. High Energy Phys.* **2013**, 490495 (2013), [arXiv:1301.0099](#).
 37. B. Müller and A. Schäfer, “Chiral magnetic effect and an experimental bound on the late time magnetic field strength”, *Phys. Rev. D* **98**, no. 7, 071902 (2018), [arXiv:1806.10907](#).
 38. D. E. Kharzeev, J. Liao, S. A. Voloshin, and G. Wang, “Chiral magnetic and vortical effects in high-energy nuclear collisions—A status report”, *Prog. Part. Nucl. Phys.* **88**, 1 (2016), [arXiv:1511.04050](#).
 39. X. Guo, J. Liao, and E. Wang, “Spin Hydrodynamic Generation in the Charged Subatomic Swirl”, *Sci. Rep.* **10**, no. 1, 2196 (2020), [arXiv:1904.04704](#).
 40. O. Vitiuk, L. V. Bravina, and E. E. Zabrodin, “Is different Λ and $\bar{\Lambda}$ polarization caused by different spatio-temporal freeze-out picture?”, *Phys. Lett. B* **803**, 135298 (2020), [arXiv:1910.06292](#).
 41. L. P. Csernai, J. I. Kapusta, and T. Welle, “ Λ and $\bar{\Lambda}$ spin interaction with meson fields generated by the baryon current in high energy nuclear collisions”, *Phys. Rev. C* **99**, no. 2, 021901 (2019), [arXiv:1807.11521](#).
 42. R.-H. Fang, L.-G. Pang, Q. Wang, and X.-N. Wang, “Polarization of massive fermions in a vortical fluid”, *Phys. Rev. C* **94**, no. 2, 024904 (2016), [arXiv:1604.04036](#).
 43. **STAR** Collaboration, C. Adler *et al.*, “Identified particle elliptic flow in Au + Au collisions at $\sqrt{s_{NN}} = 130$ GeV”, *Phys. Rev. Lett.* **87**, 182301 (2001), [arXiv:nucl-ex/0107003](#).
 44. S. A. Voloshin, “Femtoscropy of the system shape fluctuations in heavy ion collisions”, *J. Phys. G* **38**, 124097 (2011), [arXiv:1106.5830](#).
 45. **STAR** Collaboration, J. Adams *et al.*, “Pion interferometry in Au+Au collisions at $\sqrt{s_{NN}} = 200$ GeV”, *Phys. Rev. C* **71**, 044906 (2005), [arXiv:nucl-ex/0411036](#).
 46. Y. B. Ivanov and A. A. Soldatov, “Vortex rings in fragmentation regions in heavy-ion collisions at $\sqrt{s_{NN}} = 39$ GeV”, *Phys. Rev. C* **97**, no. 4, 044915 (2018), [arXiv:1803.01525](#).
 47. M. A. Lisa, J. a. G. P. Barbon, D. D. Chinellato, W. M. Serenone, C. Shen, J. Takahashi, and G. Torrieri, “Vortex rings from high energy central p+A collisions”, *Phys. Rev. C* **104**, no. 1, 011901 (2021), [arXiv:2101.10872](#).
 48. Y. Tachibana and T. Hirano, “Emission of Low Momentum Particles at Large Angles from Jet”, *Nucl. Phys. A* **904-905**, 1023c–1026c (2013), [arXiv:1210.5567](#).
 49. I. Karpenko and F. Becattini, “Study of Λ polarization in relativistic nuclear collisions at $\sqrt{s_{NN}} = 7.7 - 200$ GeV”, *Eur. Phys. J. C* **77**, no. 4, 213 (2017), [arXiv:1610.04717](#).
 50. S. Y. F. Liu and Y. Yin, “Spin polarization induced by the hydrodynamic

- gradients”, *JHEP* **07**, 188 (2021), [arXiv:2103.09200](#).
51. F. Becattini, M. Buzzegoli, and A. Palermo, “Spin-thermal shear coupling in a relativistic fluid”, *Phys. Lett. B* **820**, 136519 (2021), [arXiv:2103.10917](#).
 52. S. Y. F. Liu and Y. Yin, “Spin Hall effect in heavy-ion collisions”, *Phys. Rev. D* **104**, no. 5, 054043 (2021), [arXiv:2006.12421](#).
 53. F. Cooper and G. Frye, “Comment on the Single Particle Distribution in the Hydrodynamic and Statistical Thermodynamic Models of Multiparticle Production”, *Phys. Rev. D* **10**, 186 (1974).
 54. D. H. Rischke, “Fluid dynamics for relativistic nuclear collisions”, *Lect. Notes Phys.* **516**, 21 (1999), [arXiv:nucl-th/9809044](#).
 55. V. K. Magas, C. Anderlik, L. P. Csernai, F. Grassi, W. Greiner, Y. Hama, T. Kodama, Z. I. Lazar, and H. Stoecker, “Freezeout in hydrodynamical models in relativistic heavy ion collisions”, *Nucl. Phys. A* **661**, 596–599 (1999), [arXiv:nucl-th/0001049](#).
 56. V. Koch, S. Schlichting, V. Skokov, P. Sorensen, J. Thomas, S. Voloshin, G. Wang, and H.-U. Yee, “Status of the chiral magnetic effect and collisions of isobars”, *Chin. Phys. C* **41**, no. 7, 072001 (2017), [arXiv:1608.00982](#).
 57. F. Becattini, “Does the spin tensor play any role in non-gravitational physics?”, *Nucl. Phys. A* **1005**, 121833 (2021), [arXiv:2003.01406](#).
 58. **Particle Data Group** Collaboration, R. L. Workman *et al.*, “Review of Particle Physics”, *PTEP* **2022**, 083C01 (2022).
 59. **BESIII** Collaboration, M. Ablikim *et al.*, “Probing CP symmetry and weak phases with entangled double-strange baryons”, *Nature* **606**, no. 7912, 64–69 (2022), [arXiv:2105.11155](#).
 60. **BESIII** Collaboration, M. Ablikim *et al.*, “Precise Measurements of Decay Parameters and CP Asymmetry with Entangled $\Lambda - \bar{\Lambda}$ Pairs Pairs”, *Phys. Rev. Lett.* **129**, no. 13, 131801 (2022), [arXiv:2204.11058](#).
 61. T. D. Lee and C.-N. Yang, “General Partial Wave Analysis of the Decay of a Hyperon of Spin 1/2”, *Phys. Rev.* **108**, 1645–1647 (1957).
 62. **E756** Collaboration, K. B. Luk *et al.*, “Search for direct CP violation in nonleptonic decays of charged Ξ and Λ hyperons”, *Phys. Rev. Lett.* **85**, 4860–4863 (2000), [arXiv:hep-ex/0007030](#).
 63. **HyperCP** Collaboration, M. Huang *et al.*, “New measurement of $\Xi \rightarrow \Lambda\pi^-$ decay parameters”, *Phys. Rev. Lett.* **93**, 011802 (2004).
 64. K. B. Luk *et al.*, “New Measurements of Properties of the Ω^- Hyperon”, *Phys. Rev. D* **38**, 19–31 (1988).
 65. K.-B. Luk, *A Study of the omega- Hyperon*. PhD thesis, Rutgers U., Piscataway, 1983.
 66. J. Kim, J. Lee, J. S. Shim, and H. S. Song, “Polarization effects in spin 3/2 hyperon decay”, *Phys. Rev. D* **46**, 1060–1063 (1992).
 67. S. A. Voloshin and T. Niida, “Ultra-relativistic nuclear collisions: Direction of spectator flow”, *Phys. Rev. C* **94**, 021901(R) (2016), [arXiv:1604.04597](#).
 68. W. Florkowski and R. Ryblewski, “Interpretation of Λ spin polarization measurements”, *Phys. Rev. C* **106**, no. 2, 024905 (2022), [arXiv:2102.02890](#).
 69. **STAR Collaboration** Collaboration, J. Adam *et al.*, “Strange hadron production in Au+Au collisions at $\sqrt{s_{NN}} = 7.7, 11.5, 19.6, 27, \text{ and } 39 \text{ GeV}$ ”, *Phys. Rev. C* **102**, no. 3, 034909 (2020), [arXiv:1906.03732](#).
 70. H. Li, L.-G. Pang, Q. Wang, and X.-L. Xia, “Global Λ polarization in heavy-ion collisions from a transport model”, *Phys. Rev. C* **96**, no. 5, 054908 (2017), [arXiv:1704.01507](#).

71. X.-L. Xia, H. Li, X.-G. Huang, and H. Z. Huang, “Feed-down effect on Λ spin polarization”, *Phys. Rev. C* **100**, no. 1, 014913 (2019), [arXiv:1905.03120](#).
72. H. Li, X.-L. Xia, X.-G. Huang, and H. Z. Huang, “Global spin polarization of multistrange hyperons and feed-down effect in heavy-ion collisions”, *Phys. Lett. B* **827**, 136971 (2022), [arXiv:2106.09443](#).
73. A. H. Tang, A. H. Tang, B. Tu, A. H. Tang, C. S. Zhou, B. Tu, B. Tu, C. S. Zhou, and C. S. Zhou, “Practical considerations for measuring global spin alignment of vector mesons in relativistic heavy ion collisions”, *Phys. Rev. C* **98**, no. 4, 044907 (2018), [arXiv:1803.05777](#). [Erratum: *Phys.Rev.C* 107, 039901 (2023)].
74. P. Faccioli, C. Lourenco, J. Seixas, and H. K. Wohri, “Towards the experimental clarification of quarkonium polarization”, *Eur. Phys. J. C* **69**, 657–673 (2010), [arXiv:1006.2738](#).
75. S. Lan, Z.-W. Lin, S. Shi, and X. Sun, “Effects of finite coverage on global polarization observables in heavy ion collisions”, *Phys. Lett. B* **780**, 319–324 (2018), [arXiv:1710.03895](#).
76. **ALICE** Collaboration, S. Acharya *et al.*, “Global polarization of Λ and $\bar{\Lambda}$ hyperons in Pb-Pb collisions at $\sqrt{s_{NN}} = 2.76$ and 5.02 TeV”, *Phys. Rev. C* **101**, no. 4, 044611 (2020), [arXiv:1909.01281](#).
77. C. d. C. Barros, Jr. and Y. Hama, “Antihyperon polarization in high-energy inclusive reactions”, *Int. J. Mod. Phys. E* **17**, 371–392 (2008), [arXiv:hep-ph/0507013](#).
78. C. d. C. Barros, Jr. and Y. Hama, “ Λ and $\bar{\Lambda}$ polarization in Au-Au collisions at RHIC”, *Phys. Lett. B* **699**, 74–77 (2011), [arXiv:0712.3447](#).
79. Y. Xie, D. Wang, and L. P. Csernai, “Global Λ polarization in high energy collisions”, *Phys. Rev. C* **95**, no. 3, 031901 (2017), [arXiv:1703.03770](#).
80. Y. B. Ivanov, V. D. Toneev, and A. A. Soldatov, “Estimates of hyperon polarization in heavy-ion collisions at collision energies $\sqrt{s_{NN}} = 4$ –40 GeV”, *Phys. Rev. C* **100**, no. 1, 014908 (2019), [arXiv:1903.05455](#).
81. Y. B. Ivanov, “Global Λ polarization in moderately relativistic nuclear collisions”, *Phys. Rev. C* **103**, no. 3, L031903 (2021), [arXiv:2012.07597](#).
82. Y. Sun and C. M. Ko, “ Λ hyperon polarization in relativistic heavy ion collisions from a chiral kinetic approach”, *Phys. Rev. C* **96**, no. 2, 024906 (2017), [arXiv:1706.09467](#).
83. **STAR** Collaboration, M. S. Abdallah *et al.*, “Global Λ -hyperon polarization in Au+Au collisions at $\sqrt{s_{NN}} = 3$ GeV”, *Phys. Rev. C* **104**, no. 6, L061901 (2021), [arXiv:2108.00044](#).
84. **Particle Data Group** Collaboration, P. Zyla *et al.*, “Review of Particle Physics”, *PTEP* **2020** issue 8, no. 8, 083C01 (2020).
85. X.-G. Deng, X.-G. Huang, Y.-G. Ma, and S. Zhang, “Vorticity in low-energy heavy-ion collisions”, *Phys. Rev. C* **101**, no. 6, 064908 (2020), [arXiv:2001.01371](#).
86. A. Ayala, I. Domínguez, I. Maldonado, and M. E. Tejeda-Yeomans, “Rise and fall of Λ and $\bar{\Lambda}$ global polarization in semi-central heavy-ion collisions at HADES, NICA and RHIC energies from the core-corona model”, *Phys. Rev. C* **105**, no. 3, 034907 (2022), [arXiv:2106.14379](#).
87. Y. Guo, J. Liao, E. Wang, H. Xing, and H. Zhang, “Hyperon polarization from the vortical fluid in low-energy nuclear collisions”, *Phys. Rev. C* **104**, no. 4, L041902 (2021), [arXiv:2105.13481](#).
88. **HADES** Collaboration, R. Abou Yassine *et al.*, “Measurement of global polarization of Λ hyperons in few-GeV heavy-ion collisions”, *Phys. Lett. B* **835**, 137506 (2022), [arXiv:2207.05160](#).

89. **STAR** Collaboration, M. I. Abdulhamid *et al.*, “Global polarization of Λ and $\bar{\Lambda}$ hyperons in Au+Au collisions at $\sqrt{s_{NN}} = 19.6$ and 27 GeV”, *Phys. Rev. C* **108**, no. 1, 014910 (2023), [arXiv:2305.08705](#).
90. Y. Guo, S. Shi, S. Feng, and J. Liao, “Magnetic Field Induced Polarization Difference between Hyperons and Anti-hyperons”, *Phys. Lett. B* **798**, 134929 (2019), [arXiv:1905.12613](#).
91. Y. Jiang, Z.-W. Lin, and J. Liao, “Rotating quark-gluon plasma in relativistic heavy ion collisions”, *Phys. Rev. C* **94**, no. 4, 044910 (2016), [arXiv:1602.06580](#). [Erratum: *Phys. Rev. C* **95**, 049904 (2017)].
92. S. Ryu, V. Jovic, and C. Shen, “Probing early-time longitudinal dynamics with the Λ hyperon’s spin polarization in relativistic heavy-ion collisions”, *Phys. Rev. C* **104**, no. 5, 054908 (2021), [arXiv:2106.08125](#).
93. W.-T. Deng and X.-G. Huang, “Vorticity in Heavy-Ion Collisions”, *Phys. Rev. C* **93**, no. 6, 064907 (2016), [arXiv:1603.06117](#).
94. D.-X. Wei, W.-T. Deng, and X.-G. Huang, “Thermal vorticity and spin polarization in heavy-ion collisions”, *Phys. Rev. C* **99**, no. 1, 014905 (2019), [arXiv:1810.00151](#).
95. H.-Z. Wu, L.-G. Pang, X.-G. Huang, and Q. Wang, “Local spin polarization in high energy heavy ion collisions”, *Phys. Rev. Research* **1**, 033058 (2019), [arXiv:1906.09385](#).
96. Y. Xie, D. Wang, and L. P. Csernai, “Fluid dynamics study of the Λ polarization for Au + Au collisions at $\sqrt{s_{NN}} = 200$ GeV”, *Eur. Phys. J. C* **80**, no. 1, 39 (2020), [arXiv:1907.00773](#).
97. Z.-T. Liang, J. Song, I. Upsal, Q. Wang, and Z.-B. Xu, “Rapidity dependence of global polarization in heavy ion collisions”, *Chin. Phys. C* **45**, no. 1, 014102 (2021), [arXiv:1912.10223](#).
98. M. Baznat, K. Gudima, A. Sorin, and O. Teryaev, “Hyperon polarization in Heavy-Ion Collisions and gravity-related anomaly”, *Phys. Rev. C* **97**, no. 4, 041902 (2018), [arXiv:1701.00923](#).
99. C.-M. Ko, “Chiral kinetic modeling of vorticity and polarization”, 2020. INT workshop on Chirality and Criticality: Novel Phenomena in HIC.
100. **STAR** Collaboration, T. Niida, “Global and local polarization of Λ hyperons in Au+Au collisions at 200 GeV from STAR”, *Nucl. Phys. A* **982**, 511–514 (2019), [arXiv:1808.10482](#).
101. B. Fu, K. Xu, X.-G. Huang, and H. Song, “Hydrodynamic study of hyperon spin polarization in relativistic heavy ion collisions”, *Phys. Rev. C* **103**, no. 2, 024903 (2021), [arXiv:2011.03740](#).
102. F. Becattini, M. Buzzegoli, G. Inghirami, I. Karpenko, and A. Palermo, “Local Polarization and Isothermal Local Equilibrium in Relativistic Heavy Ion Collisions”, *Phys. Rev. Lett.* **127**, no. 27, 272302 (2021), [arXiv:2103.14621](#).
103. **STAR** Collaboration, J. Adam *et al.*, “Global polarization of Ξ and Ω hyperons in Au+Au collisions at $\sqrt{s_{NN}} = 200$ GeV”, *Phys. Rev. Lett* **126**, 162301(4, 2021) , [arXiv:2012.13601](#).
104. B. I. Abelev and others (STAR Collaboration), “Spin alignment measurements of the $K^{*0}(892)$ and $\phi(1020)$ vector mesons in heavy ion collisions at $\sqrt{s_{NN}} = 200$ GeV”, *Phys. Rev. C* **77**, 061902 (2008), [arXiv:0801.1729](#).
105. **ALICE** Collaboration, S. Acharya *et al.*, “Evidence of Spin-Orbital Angular Momentum Interactions in Relativistic Heavy-Ion Collisions”, *Phys. Rev. Lett.* **125**, no. 1, 012301 (2020), [arXiv:1910.14408](#).
106. C. Zhou, “ ϕ Meson and K^{*0} Global Spin Alignment at STAR”, *Nucl. Phys. A* **982**, 559–562 (2019).

107. **STAR** Collaboration, M. S. Abdallah *et al.*, “Pattern of global spin alignment of ϕ and K^{*0} mesons in heavy-ion collisions”, *Nature* **614**, no. 7947, 244–248 (2023), [arXiv:2204.02302](#).
108. X.-L. Sheng, L. Oliva, and Q. Wang, “What can we learn from the global spin alignment of ϕ mesons in heavy-ion collisions?”, *Phys. Rev. D* **101**, no. 9, 096005 (2020), [arXiv:1910.13684](#).
109. X.-L. Sheng, Q. Wang, and X.-N. Wang, “Improved quark coalescence model for spin alignment and polarization of hadrons”, *Phys. Rev. D* **102**, no. 5, 056013 (2020), [arXiv:2007.05106](#).
110. **ALICE** Collaboration, S. Acharya *et al.*, “Measurement of the J/ψ Polarization with Respect to the Event Plane in Pb-Pb Collisions at the LHC”, *Phys. Rev. Lett.* **131**, no. 4, 042303 (2023), [arXiv:2204.10171](#).
111. D. Shen (STAR), “Measurement of J/ψ polarization and spin alignment in Ru+Ru and Zr+Zr collisions at $\sqrt{s_{NN}} = 200$ GeV at STAR.”. 25th International Symposium on Spin Physics (SPIN2023).
112. **ALICE** Collaboration, S. Acharya *et al.*, “First measurement of prompt and non-prompt D^{*+} vector meson spin alignment in pp collisions at $\sqrt{s} = 13$ TeV”, *Phys. Lett. B* **846**, 137920 (2023), [arXiv:2212.06588](#).
113. L. Micheletti (ALICE), “Vector meson polarisation in heavy-ion collisions at the LHC.”. XXXth International Conference on Ultra-relativistic Nucleus-Nucleus Collisions (Quark Matter 2023).
114. **LHCb** Collaboration, R. Aaij *et al.*, “Measurement of the Υ polarizations in pp collisions at $\sqrt{s} = 7$ and 8 TeV”, *JHEP* **12**, 110 (2017), [arXiv:1709.01301](#).
115. **ALICE** Collaboration, S. Acharya *et al.*, “Polarization of Λ and $\bar{\Lambda}$ hyperons along the beam direction in Pb-Pb collisions at $\sqrt{s_{NN}} = 5.02$ TeV”, [arXiv:2107.11183](#).
116. **STAR** Collaboration, “Hyperon polarization along the beam direction relative to the second and third harmonic event planes in isobar collisions at $\sqrt{s_{NN}} = 200$ GeV”, [arXiv:2303.09074](#).
117. W. Florkowski, A. Kumar, R. Ryblewski, and A. Mazeliauskas, “Longitudinal spin polarization in a thermal model”, *Phys. Rev. C* **100**, no. 5, 054907 (2019), [arXiv:1904.00002](#).
118. Y. Sun and C. M. Ko, “Azimuthal angle dependence of the longitudinal spin polarization in relativistic heavy ion collisions”, *Phys. Rev.* **C99**, no. 1, 011903 (2019).
119. B. Fu, S. Y. F. Liu, L. Pang, H. Song, and Y. Yin, “Shear-Induced Spin Polarization in Heavy-Ion Collisions”, *Phys. Rev. Lett.* **127**, no. 14, 142301 (2021), [arXiv:2103.10403](#).
120. W. Florkowski, A. Kumar, A. Mazeliauskas, and R. Ryblewski, “Effect of thermal shear on longitudinal spin polarization in a thermal model”, *Phys. Rev. C* **105**, no. 6, 064901 (2022), [arXiv:2112.02799](#).
121. C. Yi, S. Pu, and D.-L. Yang, “Reexamination of local spin polarization beyond global equilibrium in relativistic heavy ion collisions”, *Phys. Rev. C* **104**, no. 6, 064901 (2021), [arXiv:2106.00238](#).
122. Y. Sun, Z. Zhang, C. M. Ko, and W. Zhao, “Evolution of Λ polarization in the hadronic phase of heavy-ion collisions”, *Phys. Rev. C* **105**, no. 3, 034911 (2022), [arXiv:2112.14410](#).
123. S. Alzhrani, S. Ryu, and C. Shen, “ Λ spin polarization in event-by-event relativistic heavy-ion collisions”, *Phys. Rev. C* **106**, no. 1, 014905 (2022), [arXiv:2203.15718](#).
124. **PHENIX** Collaboration, A. Adare *et al.*, “Measurement of the higher-order anisotropic flow coefficients for identified hadrons in Au+Au collisions at $\sqrt{s_{NN}} =$

44 *T. Niida and S. Voloshin*

200 GeV”, *Phys. Rev. C* **93**, no. 5, 051902 (2016), [arXiv:1412.1038](#).

125. J. Schukraft, A. Timmins, and S. A. Voloshin, “Ultra-relativistic nuclear collisions: event shape engineering”, *Phys. Lett. B* **719**, 394–398 (2013), [arXiv:1208.4563](#).